

OPTICAL SPECTROPOLARIMETRY OF QUASI-STELLAR OBJECTS DISCOVERED BY THE TWO-MICRON ALL SKY SURVEY¹

PAUL S. SMITH, GARY D. SCHMIDT, AND DEAN C. HINES
 Steward Observatory, The University of Arizona, Tucson, AZ 85721

AND

CRAIG B. FOLTZ
 Multiple Mirror Telescope Observatory, The University of Arizona, Tucson, AZ 85721
To appear in The Astrophysical Journal

ABSTRACT

Highly polarized QSOs discovered in the Two-Micron All Sky Survey (2MASS) have been observed to determine the source(s) of optical polarization in this near-infrared color-selected sample. Broad emission lines are observed in the polarized flux spectra of most objects, and the polarization of the lines is at about the same level and position angle as the continuum. Generally, the continuum is bluer and the broad-line Balmer decrement is smaller in polarized light than for the spectrum of total flux. Narrow emission lines are much less polarized than the broad lines and continuum for all polarized objects. These properties favor scattering by material close to a partially obscured and reddened active nucleus, but exterior to the regions producing the broad-line emission, as the source of polarized flux in 2MASS QSOs. The largely unpolarized narrow-line features require that the electrons or dust polarizing the light be located at distances from the nucleus not much greater than the extent of the narrow emission-line region. The conclusion that the scattering material is located close to the nucleus is reinforced by the observation in four objects of changes in both the degree and position angle of polarization across the broad H α emission-line profile, indicating that the broad emission-line region (BLR) is at least partially resolved at the distance of the scatterers. In addition to known high-polarization objects, four 2MASS QSOs with AGN spectral types of 1.9 and 2 were observed to search for hidden BLRs. Broad lines were detected in polarized light for two of these objects, and the polarizing mechanism appears to be the same for these objects as for the highly polarized QSOs in the sample that readily show broad emission lines in their spectra. The small observed sample of eight Type 1 2MASS QSOs has weak [O III] emission in comparison to optically-selected AGN with similar near-infrared luminosity. The observations also show that starlight from the host galaxy contributes a significant amount of optical flux, especially for the narrow-line objects, and support the suggestion that many 2MASS QSOs are measured to have low polarization simply because of dilution of the polarized AGN light by the host galaxy.

Subject headings: galaxies: active—quasars—polarization

1. INTRODUCTION

The Two-Micron All Sky Survey (2MASS; Skrutskie et al. 1997) has revealed previously unknown, primarily low-redshift active galactic nuclei (AGN) whose space density likely exceeds that of AGN selected by their ultraviolet and optical colors (Cutri et al. 2001). This large population of radio-quiet AGN was found by Cutri et al. (2001) using a simple near-IR color criterion ($J - K_s > 2$) with no regard for optical, radio, or X-ray properties. Secondary selection criteria are that the plane of the Galaxy is avoided ($|b| > 30^\circ$) to minimize the contamination of the AGN survey by reddened galactic objects, and that inclusion in the AGN sample requires detection in all three 2MASS near-IR bandpasses. The latter requirement allows for a well-defined color-selected sample, but at the expense of missing even redder AGN given the sensitivity limits of 2MASS. The color criterion ensures that known AGN (as well as stars) are not a major contaminant in the survey since the vast majority of cataloged AGN have bluer $J - K_s$ colors.

The simple selection criteria adopted by Cutri et al. (2001) result in an efficient survey for low-redshift ($z < 0.7$) AGN that are missed in surveys using traditional optical and ultraviolet search methods. Unlike UV-excess AGN samples, the 2MASS objects encompass a large range of AGN optical spectral types. Broad emission-line (Type 1), narrow emission-line (Type 2), and intermediate (Type 1.5–1.9) objects are all well-represented. Cutri et al. (2001) find $\sim 3\times$ the number of AGN showing broad emission lines in their spectra than Type 2 AGN; over the entire sky this fraction translates to nearly 6000 Type 2 AGN with $K_s \leq 15$. In addition to the red near-IR colors of the 2MASS objects, their optical faintness and red optical colors suggest that the survey is uncovering a large population of dust-obscured AGN.

Follow up X-ray observations and optical broadband polarimetry of 2MASS AGN with QSO-like near-IR luminosities support the contention that the bulk of the near-IR-selected sample is composed of objects at least partially obscured from our direct line of sight. Wilkes et al. (2002) find large absorbing columns ($N_H \sim 10^{21} - 10^{23} \text{ cm}^{-2}$) to-

¹A portion of the results presented here made use of the Multiple Mirror Telescope Observatory, a facility operated jointly by the University of Arizona and the Smithsonian Institution.

ward the nuclear X-ray sources. Smith et al. (2002) find that a large fraction ($>10\%$) of luminous 2MASS AGN ($M_{K_s} \lesssim -25$) are highly polarized ($P > 3\%$) compared to optically-selected QSOs and broad absorption-line QSOs. In fact, broadband polarizations as high as $\sim 10\%$ are measured for a few of these near-IR-selected QSOs.

In this paper, optical spectropolarimetry of all highly polarized and some moderately ($P = 1\text{--}3\%$) polarized QSOs found by Smith et al. (2002) is presented in an effort to better understand the polarizing mechanism(s) and thus place constraints on the nature of the 2MASS sample and AGN phenomena in general. In particular, it is of interest to test if the polarization properties of near-IR-selected QSOs are consistent with those found in other highly polarized AGN samples where it has been shown that much of the observational data can be explained in the terms of an obscuring dust torus surrounding the active nucleus (e.g., Antonucci 1993). For many Seyfert 2 galaxies (Antonucci & Miller 1985; Miller & Goodrich 1990; Tran, Miller, & Kay 1992), narrow-line radio galaxies (NLRGs; Tran, Cohen, & Goodrich 1995; Ogle et al. 1997; Cohen et al. 1999), and hyperluminous infrared galaxies (HIGs; see e.g., Wills et al. 1992; Young et al. 1996; Hines et al. 2001), spectropolarimetry has been able to show that orientation plays a critical role in the classification of AGN. The basic result for all of these narrow emission-line objects is that light from the active nucleus, including the ionizing continuum and the emission from the broad-line region (BLR), is obscured from direct view by dust near the nucleus, but for lines of sight that do not intersect the putative dusty torus, the nuclear radiation energizes the narrow emission-line region (NLR). Dust or electrons located within the NLR, or just outside this region, scatter some of the nuclear flux into our line of sight resulting in the detection of a blue continuum and broad emission lines in the spectrum of polarized light. Spectropolarimetry of these AGN implies that, from the vantage point of the scattering material, the Type 1 analogs to the narrow-line objects would be observed, effectively unifying apparently disparate classes of objects.

With this general picture in mind, several near-IR-selected QSOs classified as Type 2 objects were also observed to search for hidden BLRs and thereby determine if the narrow emission-line QSOs found by 2MASS are higher-luminosity analogs of Seyfert 2 nuclei. Schmidt et al. (2002) detail the results for one Type 2 2MASS QSO that reveals a hidden BLR in polarized light and shows that for at least some objects, the model that unifies Seyfert nuclei can be extended to near-IR-selected QSOs. The sample of 2MASS QSOs selected for the current study span nearly the full range of AGN spectral type, as well as a large range in broadband optical polarization. After describing the observations (§2) and the data obtained for individual objects (§3), the general trends for this optically diverse sample of QSOs are discussed in §4. We summarize our conclusions in §5. Primary among these are the findings that the polarization properties of 2MASS QSOs are consistent with these objects being obscured by dust to various degrees, and that both the obscuration and the scattering that produces the polarized flux occur near the nucleus.

2. OBSERVATIONS

Optical spectropolarimetry was obtained for 21 AGN discovered by 2MASS (Table 1) using either the 6.5 m MMT located on Mt. Hopkins, AZ, or the 2.3 m Bok Reflector on Kitt Peak, AZ. The data were acquired between 1999 October and 2002 July, providing multi-epoch sampling of several objects. All observations made use of the CCD Spectropolarimeter (Schmidt, Stockman, & Smith 1992), upgraded with a 1200×800 -pixel, thinned, antireflection-coated, UV-sensitized CCD, and an improved camera lens and half waveplate.

Data were acquired with the MMT both prior to (2001 March/April) and following the deposition of a high-quality aluminum coating on the primary mirror. The original mirror coating suffered from copper contamination that compromised reflectivity ($R \sim 40\%$ at $\lambda \sim 4000 \text{ \AA}$ and $\sim 60\%$ at $\lambda \sim 8000 \text{ \AA}$) and degraded with time. The coating also resulted in an instrumental polarization of $\sim 1\%$ that required careful calibration and removal from the 2001 March/April data through observations of several interstellar polarization and unpolarized standard stars (Schmidt, Elston, & Lupie 1992). The instrumental polarization component was reduced to $<0.1\%$ and the reflectivity increased to nearly ideal levels with the first fully successful primary mirror aluminization in 2001 November.

All observations utilized a 600 l mm^{-1} grating for high throughput and wide spectral coverage, typically $4400\text{--}8800 \text{ \AA}$. The full-width at half-maximum (FWHM) resolution with this grating and a slit width of $1''.1\text{--}3''.0$ is $\sim 17 \text{ \AA}$ (3 pixels), $\sim 800\text{--}1100 \text{ km s}^{-1}$, depending on telescope. A polarimetric measurement sequence involves four separate exposures that sample 16 orientations of the semi-achromatic half waveplate, and totals $\sim 2000\text{--}3000 \text{ s}$ of integration. Typically, 2–4 such sequences were acquired for each object in a night. Calibration of the degree of polarization (P) was made with reference to observations of an incandescent light source through a fully polarizing prism. Values quoted for P have not been corrected for Ricean statistical bias (Wardle & Kronberg 1974). In nearly all cases this correction is inconsequential for the data presented. Polarization position angles were referenced to the equatorial system by means of observations of interstellar polarization standard stars with the identical instrumental setup. The spectral flux distribution is also obtained in the course of the observations and is calibrated relative to spectrophotometric standard stars selected from the IRAF database (Massey et al. 1988). Finally, the atmospheric O_2 A and B-band absorption features, as well as the H_2O feature at $\sim 7200 \text{ \AA}$, have been removed from the flux spectra of the AGN by observing early-type stars at nearly the same airmass, or by scaling the results of the stellar observations to the features seen in the AGN spectra.

Table 1 summarizes the observations by listing the observation date, telescope, slit width, total exposure time, and the flux-weighted mean linear polarization within the $5000\text{--}8000 \text{ \AA}$ band (observed frame; unless otherwise noted, wavelengths are given in the observer's frame). In some cases more than one slit was used for an object during an observing run as dictated by conditions. Nine objects were observed during multiple epochs, and the broadband

mean polarization is listed for each observing run. There is no evidence for variability of any of these objects between epochs or between nights of a given run. The data for each object were averaged and these values are also listed in Table 1. The co-added spectropolarimetry is displayed in Figures 1, 2, and 3. The coaddition of the observations was statistically weighted by the data quality at each epoch. Because of the faintness of the targets, $16 \leq B \leq 22$, the polarization spectra can still be noisy, particularly near the limits of the spectral coverage.

2.1. The Sample of Objects

The 21 objects chosen for spectropolarimetric observation were selected from the sample 89 AGN observed by Smith et al. (2002). Seventy of these objects meet the criterion of $J - K_s > 2$ to be included in the formal sample of 2MASS red AGN (Cutri et al. 2001), and so do all but one of the spectropolarimetric targets. Because all of the 2MASS red AGN have M_{K_s} that fall comfortably within the K_s -band luminosity range of optically-selected QSOs, Smith et al. (2002) classified these objects as QSOs in their own right even though they are generally underluminous in the optical. All 10 of the QSOs found to have optical broadband polarizations $> 3\%$ by Smith et al. were selected for follow up spectropolarimetry. Of these objects, spectropolarimetry of 2MASSI J151653.2+190048 (2M151653; hereafter in the text, the identification of objects will take the form: 2Mhhmmss, where the decimal seconds of the J2000 Right Ascension have been truncated and the Declination has been omitted) and of 2M165939 using the Bok Reflector have been reported by Smith et al. (2000). We include these objects for completeness, and in the case of 2M165939, add new data obtained with the MMT.

In addition to the highly polarized QSOs in the 2MASS sample, spectropolarimetry of 2M135852 is presented. This object does not quite meet the 2MASS red AGN selection criteria with $J - K_s = 1.8$, but was found by Smith et al. (2002) to have an R -band polarization of nearly 5%.

Four 2MASS QSOs having spectra dominated by narrow emission lines (2M100121, 2M105144, 2M130005, and 2M222554) were observed ostensibly to search for broad emission lines in their polarized spectra. All of these objects have measured broadband polarizations of $< 2\%$. The positive result for 2M130005 is reported and discussed by Schmidt et al. (2002), and these data are included here for completeness and for comparison to other objects in the sample. Supplementing the observations of highly polarized and low-polarization narrow-line targets are six other 2MASS QSOs with moderate broadband polarization ($P \sim 1\text{--}3\%$). These objects were observed as time and conditions allowed.

Except for 2M004118 (§3.2.1), Galactic interstellar polarization (ISP) in the sight lines to the targets has been ignored. The high Galactic latitude of the sample and the high polarization of many of the objects virtually ensure that Galactic ISP is not a significant contributor to the observed polarization. Smith et al. (2002) directly show this to be true for six spectropolarimetry targets since only upper limits can be set for the polarization of objects near these sight lines with measurement uncertainties of $\lesssim 0.5\%$.

The high quality flux spectra that are a byproduct of the

spectropolarimetry allow a re-examination of the optical spectral classification of the 2MASS AGN that was based on the original, confirming spectroscopy (Cutri et al. 2001) listed in Smith et al. (2002). We use the AGN classification guidelines of Ho, Filippenko, & Sargent (1997) that were also used by Cutri et al. in generating the 2MASS AGN sample. This scheme is very close to the classification criteria of Veilleux & Osterbrock (1987). Some of the original classifications were ambiguous because $H\beta$ was not available for various reasons. This emission line is clearly identified in all of the 21 spectropolarimetry targets and allows for a more definitive classification of four objects. 2M135852 and 2M150113 are now classified as Type 1 AGN and 2M163700 (see Figure 2) is Type 1.5 owing to the prominent narrow-line component of $H\beta$. Schmidt et al. (2002) reclassified 2M130005 as a Type 2 AGN.

Four other objects were reclassified based on the new spectra. 2M105144 is Type 1.9 as opposed to the original LINER classification because it possesses a broad $H\alpha$ component (Figure 3). 2M222221 (Figure 2) is reclassified as Type 1.5 because of the strong, narrow emission-line component seen in the Balmer-line profiles and the relatively high ratio of $[O\ III]\lambda 5007$ to $H\beta$ flux. In contrast, the smaller $[O\ III]\lambda 5007/H\beta$ flux ratio, absence of a distinguishable narrow emission-line component for $H\beta$, and very strong optical Fe II features favor classifying 2M230307 as Type 1. The original Starburst classification is somewhat problematic for 2M100121. The emission-line ratios are consistent with either Starburst or Seyfert 2 designation, but given its high QSO-like luminosity in the near infrared, it is difficult to imagine that hot stars power the nuclear emission. Therefore, we reclassify 2M100121 as a Type 2 AGN. Table 1 summarizes the adopted AGN spectral classifications for the spectropolarimetry sample.

3. RESULTS

3.1. Spectropolarimetric Measurements

The spectropolarimetric results are presented in Figures 1–3. For all objects, the sequence of four panels depicts, from top to bottom: the polarization position angle θ , the rotated Stokes parameter q' for a coordinate system aligned with the mean polarization of the source in the 5000–8000 Å bandpass ($q' = q \cos 2\theta + u \sin 2\theta$), the polarized (or “Stokes”) flux $q' \times F_\lambda$, and finally, the total spectral flux F_λ . Two artifacts should be noted. First, even though the data have been corrected for terrestrial absorption features, the O_2 and H_2O bands are sufficiently deep that increased noise can be noted in the polarized flux spectra around the wavelengths of these features. Second, fringing sharply modulates the CCD quantum efficiency for $\lambda \gtrsim 8000$ Å. When combined with a small amount of flexure in the instrument, the result is that measured quantities show rapid oscillations as a function of wavelength around their mean values for a few objects. 2M010607 and 2M135852 (Figure 1) show examples of this effect.

Objects have been divided into three groups: Type 1, Type 1.5, and Types 1.8–2 to compare and contrast characteristics over a wide range of emission-line properties. Summarized in Table 2 are the equivalent width (EW in Å) and line flux (in units of 10^{-14} erg cm $^{-2}$ s $^{-1}$) for $H\beta$, $H\alpha$ (for objects with $z < 0.34$), and $[O\ III]\lambda 5007$. The line widths of $H\alpha$ and $H\beta$ (FWHM in km s $^{-1}$) are

also given. Because the emission lines from the NLR are generally unresolved, we do not list the [O III] λ 5007 line width, but instead tabulate the [O III] λ 5007 luminosity ($H_0 = 75 \text{ km s}^{-1} \text{ Mpc}^{-1}$, $q_0 = 0$, and $\Lambda = 0$ are assumed throughout). Measurements for all of the available quantities are given for both the total flux spectrum (F_λ) and the polarized flux spectrum ($q' \times F_\lambda$) in the observed frame. A colon after an entry signifies that the measurement is difficult and the reason for the resulting uncertainty is identified in the last column of Table 2.

Measurements of H α are contaminated to various degrees by [N II] $\lambda\lambda$ 6548,6583. The contribution to the H α flux by [N II] is not large except for the Type 1.8–2 QSOs, where the [N II] lines may emit $\gtrsim 1/2$ of the flux and broaden the feature. Flux from [S II] $\lambda\lambda$ 6717,6731 was excluded from measurements of H α + [N II]. Given the spectral resolution of the observations, the values listed in Table 2 for H α include the contributions from both the narrow and broad emission-line components as well as [N II]. Likewise, the measurements of H β include both broad- and narrow-line components of the emission feature.

Optical Fe II emission is detected in all of the Type 1 and 1.5 objects except 2M165939. Since measurements of H β and [O III] λ 5007 are affected by strong multiplets in this wavelength region, the Fe II emission was removed from F_λ and $q' \times F_\lambda$ (if detected in polarized light) before these lines were measured. An optical Fe II template based on the narrow-line QSO I Zw 1 (Boroson & Green 1992) was broadened to the approximate H β FWHM, scaled to the estimated flux of the feature observed at ~ 4450 – 4750 \AA (rest frame), and subtracted from the 2MASS QSO spectra.

The continuum properties of the 2MASS QSOs are characterized in Table 3. For more than half of the sample, a significant contribution to the observed flux is made by starlight originating in the host galaxy of the QSO. We have estimated the amount of starlight falling within the observing aperture for all objects showing stellar absorption features in their spectra. For three other objects that do not show obvious stellar features, an estimate of the host galaxy flux is provided by high resolution imaging obtained by Marble et al. (2003) using the Wide Field/Planetary Camera 2 (WFPC2) and F814W filter aboard the *Hubble Space Telescope* (HST). The elliptical galaxy spectrum of NGC 3379 (Kennicutt 1992) was used as a template to extrapolate the measured stellar contribution within the F814W filter to shorter wavelengths. This same template also reasonably accounts for the observed absorption features of the 11 objects where the host galaxy is directly detected in the total flux spectra. The ratio of starlight from the host galaxy to total flux at 5500 \AA in the rest frame is listed in Table 3, along with the polarization of the remaining light in the observed 6000 – 7000 \AA band after the subtraction of the assumed unpolarized stellar component.

Power-law fits to the continua for both the polarized flux spectrum and the host galaxy-subtracted total flux spectrum were made to characterize the continuum properties of the sample. The power-law index, β , where $F_\lambda \propto \lambda^\beta$, is given in Table 3. The power-law fits avoid regions of exceptionally high noise, major emission lines, and obvious

Fe II features if present.

Following β in Table 3 are the strengths of [O III] λ 5007, H α , and Fe II relative to the H β flux. If possible, entries for these line ratios are listed for both the total and polarized flux spectra. As in Table 2, the measurement of $F_{\text{H}\alpha}$ includes flux from [N II] $\lambda\lambda$ 6548,6583. The strength of the optical Fe II emission is characterized by the its flux within the rest frame 4450 – 4750 \AA band.

Finally, the last three columns in Table 3 list the line and continuum polarizations for H β and H α and an estimate of the polarization of the NLR based on the measurements of [O III] λ 5007. The polarizations of the permitted lines are calculated using the measured total and polarized line fluxes. The continuum polarization at H α and H β is derived from the power-law fits to the continua described above. Throughout this paper, we assume that the generally low observed polarization of the NLR is well-represented by the strength of narrow-line features in the polarized flux spectrum.

3.2. Type 1 Objects

About 3/4 of the 2MASS red AGN sample show broad emission lines in their total flux spectra (Cutri et al. 2001). In the spectropolarimetric sample, Type 1 objects correspond to those with $F_{[\text{O III}]}/F_{\text{H}\beta} < 0.5$. Spectropolarimetry of seven Type 1 2MASS QSOs and one highly polarized, broad emission-line AGN found by 2MASS (2M135852) is shown in Figure 1.

3.2.1. 2MASS J004118.7+281640

Optical unfiltered polarimetry of 2M004118 yields $P = 2.2\% \pm 0.3\%$ at $\theta = 104^\circ \pm 4^\circ$ (Smith et al. 2002). Our spectropolarimetry confirms the level of polarization, and we measure a flux-weighted polarization position angle of 97° in the 5000 – 8000 \AA bandpass. A portion of this originates as Galactic ISP, since Smith et al. (2002) found $P = 0.74\%$, $\theta = 117^\circ$ for a nearby field star. The data displayed for 2M004118 in Figure 1 and Tables 2 and 3 have been corrected for this ISP, assuming that it follows the standard Serkowski law (Serkowski, Mathewson, & Ford 1975) with a maximum polarization of 0.74% at 5500 \AA .

Although the polarization of 2M004118 is diminished by the ISP correction, it is clear that the object is intrinsically polarized. The spectrum of q' shows that the H α , H β , and [O III] emission lines are not polarized to the same degree as the surrounding continuum, as would be expected if ISP were the sole polarizing mechanism. The ISP correction yields a mean polarization in the 5000 – 8000 \AA bandpass for 2M004118 of $P \sim 1.7\%$ at $\theta \sim 89^\circ$.

2M004118 is one of the bluest objects in the sample, with $B - K_s = 3.4$ and $\beta_{F_\lambda} = -2.2$, and has strong optical Fe II emission features. The polarized flux spectrum shows a continuum nearly as blue as the total flux spectrum. Hydrogen α exhibits changes in q' and θ across its profile. The core of the line marks a transition between the red wing of the line that is polarized to the degree and position angle of the continuum, and the less polarized blue wing. The position angle swings through $\sim 90^\circ$ near the line core. A similar signature in q' is identified for H β and the strong Fe II feature blended with [O III] λ 5007 at 5980 \AA . The complex structure of the H α polarized flux profile is reminiscent of some highly polarized Seyfert 1

nuclei (e.g., Goodrich & Miller 1994; Smith et al. 1995, 1997; Martel 1997, 1998; Smith et al. 2002).

3.2.2. 2MASS J010607.7+260334

In contrast to 2M004118, 2M010607 is a much redder object optically ($\beta_{F_\lambda} = 1.3$; $B - K_s > 6$), more than 3 mag fainter, and more highly polarized. 2M010607 shows Fe II emission features nearly as strong relative to H β as in 2M004118. Unfortunately, the redshift of 2M010607 places H α outside the sensitivity range of the spectropolarimeter. The primary feature of the polarized flux spectrum is the presence of broad (~ 1900 km s $^{-1}$ FWHM) H β with roughly the same equivalent width as seen in the total flux spectrum. There is no evidence of [O III] $\lambda 5007$ in the polarized flux spectrum and the polarized continuum is quite red ($\beta_{q' \times F_\lambda} = 0.5$).

3.2.3. 2MASS J125807.4+232921

Spectropolarimetry of 2M125807 confirms the low R -band polarization measurement reported in Smith et al. (2002). The object is $\sim 1\%$ polarized and the appropriate quantities listed in Table 3 have been measured after subtracting an elliptical host galaxy spectrum that accounts for 13% of the total light received at 5500 Å in the rest frame. Because stellar spectral features are not apparent in the spectrum, the contribution of the host galaxy was estimated from an *HST* WFPC2 F814W image (Marble et al. 2003). In this case, the host galaxy has little impact on the measured polarization and other quantities.

The spectral slopes of total flux and polarized flux continua are similar to those of 2M004118, as is the Balmer decrement in the total flux spectrum. Subtraction of the Fe II template from the total flux spectrum accounts for all of emission peaks between H β and ~ 7000 Å. There is no evidence of [O III] emission from 2M125807, making this the only object in spectropolarimetric sample not exhibiting emission lines from this species. No definitive features are seen in the polarized flux spectrum.

3.2.4. 2MASS J132917.5+121340

Although 2M132917 is polarized only $\sim 1\%$ around H α , its polarization rises rapidly to the blue. Indeed, the object exhibits one of the bluest polarized flux spectra of this sample ($\beta_{q' \times F_\lambda} = -2.0$), much bluer than the total flux continuum ($\beta_{F_\lambda} = -0.5$). The feature seen in the polarized flux spectrum near [O III] $\lambda 5007$ is much narrower (~ 1 pixel) than the instrumental resolution and could simply be a noise spike due to a cosmic ray. The flux in this narrow feature is used as an upper limit to the polarized flux from [O III] $\lambda 5007$. Comparison of the H β /[O III] $\lambda 5007$ flux ratio for both F_λ and $q' \times F_\lambda$ suggests that the polarization of the BLR is at least four times higher than that of the NLR.

The Balmer lines reveal a pronounced red asymmetry in their profiles in the total flux spectrum. Much like 2M004118, the H α polarized flux is emitted in the red wing of the line. Near the line core and in the blue wing q' falls well below 0. Since there is no corresponding feature seen in the rotated u Stokes parameter, the polarization of the blue wing of H α is orthogonal to that of the red wing. The two polarized components would then tend to cancel near the line core, as seen in the q' and $q' \times F_\lambda$

panels for 2M132917 in Figure 1. The line center of H β in polarized flux is shifted ~ 1000 km s $^{-1}$ to the red of the line peak in total flux. This could be caused by the same polarization structure seen in H α , although the spectropolarimetry does not have the signal-to-noise ratio (S/N) to clearly show these features.

3.2.5. 2MASS J135852.5+295413

This object is not a member of the 2MASS red QSO sample because $J - K_s = 1.8$ in revised 2MASS photometry. Nevertheless, 2M135852 has a K_s luminosity well within the range of the 2MASS QSOs and $B - K_s = 4.15$, redder than the median $B - K_s$ color index of the Type 1 objects observed by Smith et al. (2002). In addition, R -band imaging polarimetry shows $P \sim 4.8\%$, resulting in the object being added to the list of 2MASS AGN for follow up observation.

Spectropolarimetry confirms the highly polarized nature of 2M135852. The polarization reaches $\sim 8\%$ at 4600 Å and has a position angle that is constant with wavelength. The spectrum reveals stellar absorption features that can be removed with a starlight fraction of $\sim 60\%$ in the observing aperture at 5500 Å (rest frame). This implies an intrinsic polarization in the 6000–7000 Å band double of that observed, and well over 10% for $\lambda < 5000$ Å. The host galaxy also leads to higher observed polarization in the Balmer lines than in the continuum since the relative dilution in the lines is reduced. Balmer line widths in F_λ and $q' \times F_\lambda$ are about the same. Even with the correction to F_λ for a red stellar component, the polarized flux continuum is bluer than the nuclear light in the total flux spectrum.

The q' panel in Figure 1 for 2M135852 indicates that the polarization at [O III] $\lambda 5007$ is much diminished from the surrounding continuum. Estimating the [O III] $\lambda 5007$ flux in the polarized spectrum yields a polarization for the NLR of $\lesssim 2.5\%$. Unlike several other Type 1 objects, 2M135852 shows no structure in θ across H α in the polarized flux spectrum.

3.2.6. 2MASS J150113.1+232908

2M150113 is optically the reddest of the eight Type 1 objects with $\beta_{F_\lambda} = 2.3$, and the Ca II H and K break is seen in its spectrum. The stellar features imply that the host galaxy contributes $\sim 60\%$ of the light at 5500 Å (rest frame) within the $1''.5 \times 3''.8$ observation aperture. This, in turn, suggests that the polarization of the nuclear light in the R -band is $\sim 8\%$, in contrast to the $P = 3\text{--}4\%$ measured by the spectropolarimetry and by Smith et al. (2002). The increased polarization seen at H α and H β is explained by unpolarized starlight included in the aperture, as is also the case for 2M135852.

The noise level of the polarized flux spectrum makes it difficult to determine if [O III] $\lambda 5007$ is present in polarized light. An upper limit to the [O III] $\lambda 5007$ polarized flux suggests that the emission from the NLR cannot be polarized more than $\sim 1/3$ of the polarization measured for the continuum and BLR.

The degree of polarization of 2M150113 rises to the blue as indicated by the spectral index of the polarized continuum relative to the total nuclear continuum (after the host galaxy spectrum has been subtracted). In addition,

the Balmer decrement is large in both the total flux spectrum ($F_{H\alpha}/F_{H\beta} \sim 12$) and the the polarized flux spectrum ($F_{H\alpha}/F_{H\beta} \sim 7$). The large decrement in $q' \times F_{\lambda}$ indicates that that even the light scattered into our view is substantially reddened.

3.2.7. *2MASS J151653.2+190048*

Smith et al. (2000) describe the polarization properties of this object. We include it here to compare with the rest of the sample and to tabulate the measurements listed in Tables 2 and 3. The object is the most luminous at K_s of the Type 1 QSOs in the spectropolarimetry sample.

The strong optical Fe II emission features are observed in the spectrum of polarized flux at about the same strength relative to H β as in the total flux spectrum. The only other QSO in this sample to unambiguously show polarized Fe II features is 2M091848 (see §3.3.1). The broad emission lines are polarized at about the same level as the continuum, which exhibits a strong rise in polarization from 8600 Å ($P \sim 7\%$) to 4600 Å ($P \sim 14\%$). The bluer polarized flux spectrum relative to the total flux spectrum is accompanied by a Balmer decrement in polarized light nearly a factor of 2 smaller than for the total flux spectrum.

The NLR is unpolarized as indicated by the absence of [O III] $\lambda\lambda 4959, 5007$ in the polarized flux spectrum. Structure is observed in q' and θ across H α , and to a lesser degree, H β (Figure 1). The red wings of the Balmer lines are more highly polarized than the blue wings. This same signature is seen for H α in the Type 1 objects 2M004118 and 2M132917.

3.2.8. *2MASS J230307.2+254503*

This object is the strongest Fe II emitter relative to H β of the QSOs in this sample. Unfortunately, H α falls very close to the red end of the spectrum, making measurements of this emission line somewhat problematic. The S/N of the spectropolarimetry is too low around the H α line for any meaningful measurements. Despite the faintness of this QSO and its relatively low optical polarization, H β can be seen in emission in polarized flux. Another feature apparent in Figure 1 is the decline of polarization to $q' \sim 0$ at [O III] $\lambda 5007$.

3.3. *Intermediate Objects*

In this section we discuss QSOs classified as Type 1.5. The narrow line-dominated Type 1.8 and 1.9 objects, also considered “intermediate” AGN spectral types, have been lumped together with the Type 2 2MASS QSOs (§3.4). This division also separates objects in the sample by their [O III] $\lambda 5007$ /H β flux ratios, with Type 1.5 QSOs in this sample having $0.5 \leq F_{[O III] \lambda 5007}/F_{H\beta} \leq 3$. Figure 2 displays the results for these objects.

3.3.1. *2MASS J091848.6+211717*

The polarization of 2M091848 increases strongly to the blue, reaching over 10% for $\lambda < 5000$ Å, and has a position angle that is constant with wavelength. The Balmer lines, including H γ , are seen in polarized flux, as is [O III] $\lambda 5007$.

2M091848 along with 2M151653 are the only two objects to clearly show polarized optical Fe II emission features.

The Fe II emission on either side of H β in 2M091848 is more prominent in polarized flux than in the total flux spectrum largely because of the significant amount of host galaxy starlight included in the total flux. Stellar absorption features in F_{λ} suggest a stellar-to-total light ratio at 5500 Å (rest frame) of ~ 0.4 . This contribution by the host galaxy implies that the intrinsic R -band polarization of the QSO is $\sim 10\%$, as opposed to $6.3 \pm 0.1\%$ measured by Smith et al. (2002) without correction for starlight.

The polarized flux spectrum of 2M091848 shows [O III] $\lambda 5007$, though its strength relative to H β is much reduced and the weaker [O III] $\lambda 4959$ line does not rise above the S/N level in polarized light. The [O III] $\lambda 5007$ measurements yield a polarization for this line of $\sim 2\%$, which is a factor of 4–6 lower than the polarization of H β and the continuum at this wavelength.

3.3.2. *2MASS J134915.2+220032*

2M134915 is the least luminous QSO in the sample in the near infrared ($M_{K_s} = -24.9$) and has the smallest near-IR-to-optical flux ratio inferred from $B - K_s$. Although the observed polarization for 2M134915 is much lower than in 2M091848, many of the polarization properties of these two QSOs are similar. Both exhibit redder continua in total flux than in polarized flux. Both objects clearly show a polarized [O III] $\lambda 5007$ line. In 2M134915, [O III] $\lambda 4959$ is also seen in $q' \times F_{\lambda}$. Based on the [O III] measurements, the NLR is polarized by $< 1\%$; $< 1/4$ the polarization of the continuum at this wavelength.

Unlike most of the Type 1 objects, which typically show Balmer lines in polarized light that have about same FWHM as in total flux, polarized H β in 2M134915 has a width ~ 2700 km s $^{-1}$ larger than measured in the total flux spectrum. To a large extent, this reflects the lessened contribution from the NLR in the polarized H β line profile compared to that for the line in total flux. The increased polarization seen in the Balmer lines is caused by the substantial contribution from the host galaxy within the observing aperture. From the stellar features observed in the spectrum, nearly half of the light within the aperture at 5500 Å (rest frame) is starlight from the host galaxy.

3.3.3. *2MASS J163700.2+222114*

The Ca II H and K break is readily apparent in the spectrum 2M163700. The stellar features imply a flux contribution by the host galaxy of ~ 0.5 at 5500 Å (rest frame) that in turn suggests an intrinsic level of polarization of the AGN of over 4%. Although the continuum slope of the polarized flux spectrum is bluer than that of the total flux, both are red ($\beta_{F_{\lambda}} \sim 2.0$; $\beta_{q' \times F_{\lambda}} \sim 0.9$). Large Balmer decrements in both polarized and total flux spectra further confirm the highly reddened nature of this QSO. In fact, these decrements are by far the largest for the Type 1.5 QSOs, and only 2M150113 challenges 2M163700 in this parameter among the Type 1 objects. There is no evidence for [O III] (or [O II] $\lambda 3727$) in the polarized flux spectrum.

3.3.4. *2MASS J165939.7+183436*

Spectropolarimetry of this object obtained at the Bok Reflector is reported and discussed by Smith et al. (2000). Subsequently, an MMT observation of similar quality was obtained of 2M165939 on 2001 March 31. No significant

differences are seen between these observations and the co-added results from the two telescopes are displayed in Figure 2. Like 2M134915 and 2M163700, the host galaxy of 2M165939 contributes to the observed flux. Various slit widths ($1''$ – $3''$) were employed for the observations of 2M165939 and a starlight-to-total flux ratio of 0.26 in the rest frame V -band is adopted for the composite spectrum. This ratio is based on the identification of a weak absorption feature at ~ 6060 Å with Mg I b.

Narrow emission lines seen in the total flux spectrum are not seen in polarized light. In contrast, $H\alpha$ and $H\beta$ are prominent in the polarized spectrum and are much broader than in either F_λ or $q' \times F_\lambda$ for any of the Type 1 objects. The asymmetric profile of the broad component of $H\alpha$ in the total flux spectrum is somewhat reproduced in polarized light with the blue wing of the line being sharper than the red wing. The broad hump identified with $H\beta$ in the polarized spectrum has an impressive FWHM of nearly $16,000 \text{ km s}^{-1}$.

3.3.5. 2MASS J170003.0+211823

2M170003 has the highest redshift, $z = 0.596$, of the 2MASS QSOs and is one of the reddest objects in the sample. It also shows the highest observed optical broadband polarization ($P \sim 11\%$; Smith et al. 2002). The spectropolarimetry confirms the high level of polarization and reveals that the polarized spectrum is about as red as the extremely red continuum observed in total light. Again, the major difference between the spectra of total and polarized light is that the emission from the NLR region is absent in the polarized flux spectrum. Broad $H\beta$ and $H\gamma$ are detected in polarized spectrum and are polarized to about the same degree as the continuum. The position angle is constant across the entire spectrum.

3.3.6. 2MASS J222202.2+195231

The highly polarized QSO 2M222202 is the most luminous ($M_{K_s} = -28.6$) of the sample of 70 2MASS red QSOs observed by Smith et al. (2002) and it displays a very rich emission-line spectrum that includes emission lines of H, He I, He II, O III, [O II], [O III], [Ne III], [Ne V], and [S II] (Figures 2 and 4). Weak optical Fe II features are also present. Remarkably, with the possible exception of $H\beta$, none of these features are seen in the polarized flux spectrum. The rotated Stokes parameter shows complex structure across the spectrum with dramatic decreases in polarization at each emission line. Indeed, significant decreases in q' are even seen at the locations of lines with small equivalent widths, such as He II $\lambda 4686$ and [O II] $\lambda 3727$. The continuum polarization increases from $\sim 10\%$ at the red end of the spectrum to nearly 18% at ~ 5370 Å, in the gap between He and [Ne III] $\lambda 3869$ + He I $\lambda 3889$ + H ζ . The continuum polarization then decreases from this point until the blue end of the observed spectrum at 4200 Å where q' is again $\sim 10\%$.

The position angle spectrum is not as dramatic as q' , but is of sufficient S/N to show interesting structure as well (Figure 4). Generally from ~ 5600 Å to 8600 Å, θ is nearly constant at around 120° . However, a 10° rotation can be seen at the location of [O III] $\lambda 5007$ and more tentatively in the core of $H\beta$ and at $H\gamma$ + [O III] $\lambda 4363$. A smaller rotation in the same sense can be discerned at

[O III] $\lambda 4959$. Although q' is based on a position angle of 120° , these $\lesssim 10^\circ$ rotations in θ are too small to significantly affect the spectrum of q' presented in Figure 4.

In addition to the discrete rotations in θ in some of the emission lines, a broad feature is observed centered near 5000 Å. The rotation has about the same amplitude as seen for [O III] $\lambda 5007$, and although the S/N is much diminished at the blue end of the spectrum, θ appears to recover back to $\sim 120^\circ$ by 4400 Å. This feature coincides with the decrease in the continuum polarization in the blue and the emergence of the “ 3000 Å bump” in the flux spectrum (see e.g., Wills, Netzer, & Wills 1985). At these wavelengths, the 3000 Å bump is primarily emission from high-level Balmer lines and the Balmer continuum. In 2M222202, this feature, [O III] $\lambda \lambda 4959, 5007$, and other emission lines must be polarized since θ cannot be affected by unpolarized light. The continuum is polarized to a much higher degree than the emission from the NLR since the rotation in θ at strong NLR features is only $\sim 10^\circ$. Measurement of the [O III] $\lambda 5007$ line implies a polarization for the NLR light of $P \sim 0.8\%$ at $\theta \sim 85^\circ$. Assigning the same polarization to the 3000 Å bump does not readily account for the polarization observed near the Balmer limit, although the decomposition of the spectrum into two polarized components is highly dependent on uncertain choices of the continuum strength and polarization in this spectral region. To be consistent with the results at [O III] $\lambda 5007$, either the 3000 Å bump must be a larger contributor to the total flux around 5000 Å than implied by a simple extrapolation from longer wavelengths, or the continuum polarization at ~ 5000 Å is not as high as indicated by the rapid rise in P observed at longer wavelengths.

The deviations in θ across the spectrum make it more difficult to interpret the spectrum of polarized light. The emission lines seen in F_λ are absent in $q' \times F_\lambda$. There is an abrupt break in the polarized flux spectrum around $H\beta$ /[O III] $\lambda \lambda 4959, 5007$ where the continuum flattens from $\beta_{q' \times F_\lambda} \sim -2.3$ for $\lambda \gtrsim 6800$ Å to $\beta_{q' \times F_\lambda} \sim -0.4$ for $\lambda \lesssim 6800$ Å. A very low contrast emission feature is tentatively identified at the location of $H\beta$ and [O III] $\lambda \lambda 4959, 5007$. If this feature is actually polarized flux from $H\beta$, the line is polarized at only $\sim 1/2$ the level of the continuum. An identification with $H\beta$ also implies that the scattered line profile is even broader ($\sim 17,000 \text{ km s}^{-1}$ FWHM) than the polarized $H\beta$ profile observed in 2M165939 (§3.3.4). The “feature” could also simply be a manifestation of the position angle rotation seen in the emission lines. We have included measurements of the feature in Tables 2 and 3 under the assumption that it is $H\beta$.

The ambiguity in the identification of polarized $H\beta$, and the lack of other lines in the polarized flux spectrum of 2M222202, results in greater uncertainty in identifying the mechanism responsible for the high continuum polarization. The polarization of the narrow emission-lines must either be caused by scattering from material far enough away from the NLR to result in a net polarization of the light, or dichroic absorption in the sight line between us and the NLR of 2M222202. Dichroic absorption is essentially ruled out as the cause of the continuum polarization because an enormous amount of extinction would be required to account for polarization approaching 20% . Scattering by dust or electrons requires that the particles be

located very close to the nuclear continuum source. To account for the very weak (or nonexistent) broad-line features in the polarized flux, the scatterers need to be intermixed with the gas in the BLR, or located just exterior to the line-emitting region. Polarized flux produced in such close proximity to the BLR probably favors electrons as the scatterers since the environment is likely to be too harsh for the survival of dust grains (however, see e.g., Goodrich 1995 for evidence that dust can exist in the BLR).

If indeed the polarized flux spectrum of 2M222202 is featureless, synchrotron radiation is a possible source of the highly polarized continuum. In this case, the optical flux and polarization would be expected to strongly vary as observed for OVV quasars and BL Lacertae objects. In fact, there is no evidence for variability in 2M222202 from the three epochs of spectropolarimetry obtained between 1999 September and 2002 July. 2M222202 is detected as a 5 mJy radio source at 1.4 GHz in the NRAO VLA Sky Survey (Condon et al. 1998), but the object is $\sim 100 - 1000\times$ less luminous in the radio than objects that show strong and variable optical synchrotron continua.

3.3.7. 2MASS J222221.1+195947

The polarization of 2M222221 is only $\sim 1\%$ even after subtracting the host galaxy contribution to the observed spectrum estimated from *HST* imaging (Marble et al. 2003, $F_{\text{gal}}/F_{\text{Total}} \sim 0.3$ in the rest frame V-band). Despite the low level of polarization, broad $H\alpha$ and $H\beta$ are apparent in $q' \times F_{\lambda}$. The lines in polarized flux are blue-shifted by $\sim 1000 \text{ km s}^{-1}$ relative to the narrow Balmer-line components in the total flux spectrum. Also detected in the polarized flux is $[\text{O III}]\lambda 5007$, although at a reduced strength relative to $H\beta$. This yields an estimate of the NLR polarization of only $\sim 0.3\%$. One other feature of note for 2M222221 is a large rotation in θ across $H\alpha$. The position angle is $\sim 160^\circ$ in the blue wing of the line, $\sim 180^\circ$ around the line core, and then rotates to $130^\circ - 110^\circ$ in the red wing.

3.4. Type 1.8, 1.9, and 2 Objects

The objects described in this section would traditionally not be classified as QSOs on the basis of their optical spectra since their narrow emission lines far outshine any weak broad permitted lines. Indeed, their $H\beta$ widths are $\sim 1000 \text{ km s}^{-1}$ (FWHM) or less. All but one show stellar absorption features with equivalent widths suggesting that well over half of the optical continuum flux is starlight from the galaxy hosts. The 2MASS results tell a much different story for these red QSOs: all have $M_{K_s} < -25.5$ and have large near-IR/optical flux ratios ($B - K_s > 5$). Spectropolarimetry of the Type 1.8–2 QSOs is displayed in Figure 3.

Combining the Type 1.8–2 objects separates QSOs with $F_{[\text{O III}]} / F_{H\beta} > 3$ from the rest of the sample. Their total flux spectra generally have larger Balmer decrements than those measured for the Type 1s and 1.5s. This is due in part to the inclusion of $[\text{N II}]\lambda\lambda 6548, 6563$ in the spectral measurements of $H\alpha$, since the $[\text{N II}]$ flux in several objects is comparable to $H\alpha$. The presence of the $[\text{N II}]$ lines also yields widths in total flux that are roughly double those measured for $H\beta$. Optical Fe II emission is not detected in these six objects.

3.4.1. 2MASS J010835.1+214818

2M010835 is the only object besides 2M171559 (§3.4.5) among the 15 Type 1.8–2 AGN in the 2MASS red QSO sample that shows broadband optical polarization $> 3\%$ (Smith et al. 2002). Spectropolarimetry confirms that the polarization of the continuum is $\sim 5\%$ and reveals stellar features in the total flux spectrum. The strength of the features suggests that about 80% of the continuum at $\sim 7000 \text{ \AA}$ is starlight, requiring that the true continuum polarization of the AGN be over 20% redward of $[\text{O III}]\lambda 5007$ and $< 10\%$ at the blue end of the spectrum. However, given the faintness of the continuum, this estimate is very uncertain. A fainter host galaxy would, of course, result in lower overall polarization as well as a smaller relative decrease in the polarization in the blue since the spectrum of the AGN would be redder.

Permitted and forbidden lines are observed in the polarized flux spectrum. Although $H\alpha$ is near the red end of the observed spectrum where the S/N is low, the line (plus possibly $[\text{N II}]$) can be seen in polarized flux. Both $[\text{O III}]$ lines are apparent in $q' \times F_{\lambda}$, but at much smaller equivalent widths than in total flux. The ratio of the polarized-to-total $[\text{O III}]$ flux implies a polarization of $\sim 1.5\%$, substantially less than for the continuum. Relative to $[\text{O III}]$, the Balmer lines are stronger in polarized light than in F_{λ} , indicated a higher polarization for the permitted lines.

3.4.2. 2MASS J100121.1+215011 and 2MASS J222554.2+195837

The Type 2 QSOs 2M100121 and 2M222554 are polarized at a very low level ($< 1\%$) and no features can be discerned in the spectrum of polarized light. Stellar absorption features in the total flux spectra, including the Ca II break, indicate that the host galaxy contributes $\sim 80\%$ of the light from these objects at 5500 \AA (rest frame) within the $1''.1 \times \sim 4''$ apertures employed for the spectropolarimetry. Correcting the data for even this large amount of unpolarized flux only elevates the polarization of 2M222554 to $\sim 1\%$.

3.4.3. 2MASS J105144.2+353930

2M105144, like 2M100121 and 2M222554, is not highly polarized and exhibits prominent stellar features in its spectrum. The ratio of starlight to AGN light in the $1''.5 \times 4''.6$ aperture used is estimated to be ~ 2.3 in the rest-frame V-band. Subtraction of the assumed elliptical galaxy spectral template gives an *R*-band polarization of 2–3% for the remaining light.

Measurements of $H\alpha$ reported in Tables 2 and 3 are uncertain because the redshift places the line center at the position of the O_2 A-band absorption. Despite this unfortunate coincidence, 2M105144 earns its classification of Type 1.9 because $H\alpha$ possesses an $\sim 18,000 \text{ km s}^{-1}$ (full width at zero intensity) component. This broad feature is also detected in the polarized flux spectrum, indicating that some of the flux from the inner BLR is scattered into our line of sight. No other features are identified in the polarized spectrum.

3.4.4. 2MASSI J130005.3+163214

Schmidt et al. (2002) present and discuss the MMT observations of the Type 2 QSO 2M130005 that are redisplayed in Figure 3. The dominant feature in the polarized spectrum of 2M130005, as for 2M105144, is very broad ($\sim 18,000 \text{ km s}^{-1}$ FWHM) $H\alpha$. The S/N of the data is much higher than for 2M105144, and Schmidt et al. (2002) are able to deduce the polarization of the continuum, broad $H\alpha$, and the narrow emission lines. In comparison to other QSOs in the sample, 2M130005 has by far the reddest total flux (after subtracting the substantial contribution of the host galaxy) and polarized flux spectra. Not all of the Na I D feature is stellar in origin, since it can be seen in $q' \times F_\lambda$.

In addition to the red polarized continuum, the Balmer decrement is possibly very large since $H\beta$ is not definitively detected in polarized flux. However, assuming that $H\beta$ is as broad as $H\alpha$ in polarized flux, the extreme width of the line hinders its identification. A rough limit on the strength of a possible broad $H\beta$ feature was estimated by fitting a power-law to the polarized continuum redward of 5900 \AA and avoiding $H\alpha$. Subtraction of this fit from $q' \times F_\lambda$ reveals emission from $\sim 5700 \text{ \AA}$ to the blue edge of the spectrum at 4200 \AA that could be the broad, blended lines of $H\beta$, $H\gamma$, and higher-order Balmer lines. The possible emission excess may indicate that the $H\beta$ flux is as much as $0.14 \times 10^{-14} \text{ erg cm}^{-2} \text{ s}^{-1}$, implying a polarized Balmer decrement of only ~ 3 .

3.4.5. 2MASSI J171559.7+280717

This object is the most distant of the Type 1.8–2s and one of the most luminous QSOs in the sample ($M_{K_s} = -28.1$). Its redshift of $z = 0.524$ has shifted $H\alpha$ out of the observed spectral range. Weak, broad $H\beta$ is detected and we therefore classify 2M171559 as Type 1.8.

The object is extremely faint ($V \sim 21.4$), but the spectropolarimetry confirms that 2M171559 does indeed join 2M010835 in showing a broadband polarization $> 3\%$. Marble et al. (2003) find significant extended flux around the AGN in the WFPC2 F814W image. Using this observation to estimate the contribution of starlight in the spectropolarimetry suggests that about half of the light at a rest frame wavelength of 5500 \AA is from the host galaxy. This choice of host galaxy is quite uncertain as there are no discernible stellar features superimposed on the faint continuum. A host galaxy contribution this large implies an intrinsic polarization within the R -band of over 15% for the AGN.

There is no evidence of the strong, narrow emission lines in the polarized flux spectrum. Close inspection of the spectrum of q' reveals decreases in the polarization at $[\text{O III}]\lambda\lambda 4959, 5007$, $[\text{O II}]\lambda 3727$, and the narrow component of $H\beta$. Some of the increase in polarized flux between the location of narrow $H\beta$ and the $[\text{O III}]$ lines could be due to polarized broad $H\beta$. The S/N is insufficient to unambiguously identify broad $H\beta$ in polarized light and we have not attempted to measure the width and strength of this possible feature. Although the measurements are uncertain, the polarized flux continuum (ignoring the region around $H\beta$) is much redder than that of the host galaxy-subtracted total flux.

4. DISCUSSION

4.1. Spectral Properties

Although nearly the full range of AGN spectral types is represented by the 21 objects described in the previous section, they may not be representative of the 2MASS AGN sample as a whole. The objects chosen for observation are primarily highly polarized. This bias translates into a sample that is generally more luminous in the near-IR and has higher near-IR-to-optical flux ratios than a “typical” 2MASS QSO (Smith et al. 2002). Caution should therefore be exercised in extrapolating the spectroscopic results for the highly polarized objects to the entire sample. The 2MASS sample is generally compared to the low-redshift ($z < 0.6$) members of the Palomar-Green (PG) QSO sample (Schmidt & Green 1983) in the following discussion. The choice of the PG sample to represent optically-selected QSOs is primarily dictated by the large amount of data available in the literature for these objects.

4.1.1. $[\text{O III}]\lambda 5007$ Luminosity

The 2MASS AGN discussed in the previous section have been classified as QSOs based on the fact that they are as luminous at $2.2 \mu\text{m}$ as QSOs in other samples, not because of their observed optical luminosity or color. Indeed, nearly half of the spectropolarimetry sample shows evidence that starlight from the host galaxy contributes more than 50% of the continuum light observed in the $1''$ – $3''$ apertures employed. The red colors and high fraction of optical host galaxy starlight are consistent with the nuclear regions being obscured and reddened by dust in our line of sight, resulting in a QSO sample that is apparently optically underluminous and redder than previous cataloged QSOs. The high polarizations observed in the 2MASS sample are also consistent with a sample of objects partially hidden from direct view by dust (Smith et al. 2002). Since the dust extinction at K is much less than that experienced at optical wavelengths, it stands to reason that a near-IR search would uncover QSOs missed by surveys that rely on optical color and luminosity selection criteria, and that the intrinsic luminosity of these AGN would be more accurately estimated from a near-IR brightness than by optical magnitude.

Data at longer wavelengths offer some support for the assumption that the absolute K_s magnitude, M_{K_s} , can be used to distinguish QSOs from AGN of lower luminosity (Smith et al. 2002). Of the objects detected at $60 \mu\text{m}$ and 1.4 GHz , there is no large systematic difference between 2MASS QSOs and optically-selected QSOs for a given $2.2 \mu\text{m}$ luminosity. The validity of using M_{K_s} as a measure of intrinsic luminosity can also be verified optically by inspecting the $[\text{O III}]\lambda 5007$ luminosities. In the context of current ideas on the role that viewing orientation plays in determining the observed properties of AGN (see e.g., Antonucci 1993), emission from the kpc-sized NLR is generally thought to be more isotropic than the emission from the BLR and ionizing continuum, although there is evidence for anisotropy in at least the higher ionization narrow emission lines in some AGN (see e.g., Jackson & Browne 1990; Hes, Barthel, & Fosbury 1993; Baker 1997). Despite these examples, the $[\text{O III}]\lambda 5007$ flux should, to first order, scale with the luminosity of the ionizing nuclear continuum.

Figure 5 compares the $[\text{O III}]\lambda 5007$ luminosity of the 2MASS spectropolarimetry sample with low-redshift PG QSOs. Following Boroson & Green (1992), the $[\text{O III}]\lambda 5007$ luminosity is given by

$$M_{[\text{O III}]} = M_V - 2.5 \log(\text{EW}_{[\text{O III}]}) ,$$

where M_V is calculated from the rest frame 5500 Å flux density. For both samples of objects, a clear trend of increasing $[\text{O III}]\lambda 5007$ luminosity with increasing M_{K_s} is seen. In addition, the strength of the $[\text{O III}]\lambda 5007$ emission from the 2MASS QSOs is within the large range exhibited by the optically-selected QSOs. For the predominantly highly polarized 2MASS sample, the Type 1.5, 1.8 (2M171559), and 1.9 (2M010835) objects cannot be distinguished from the low-polarization, Type 1 PG QSOs. The three Type 2 QSOs and 2M105144 are clustered around $M_{K_s} \sim -26$, $M_{[\text{O III}]} \sim -24.5$; consistent with PG QSOs in having fainter $[\text{O III}]$ emission for this lower near-IR brightness.

It is true that, in comparison with the PG sample, the Type 1 2MASS QSOs typically have a lower $[\text{O III}]$ luminosity for a given brightness at K_s . Only seven of the eight Type 1 QSOs are included in Figure 5 since $[\text{O III}]\lambda 5007$ is not detected in 2M125807. Such weak $[\text{O III}]$ is also seen in some PG QSOs, as four of 74 objects in the Boroson & Green (1992) study do not show emission from the NLR, and there are some PG QSOs with $[\text{O III}]$ strengths as low as the 2MASS objects. However, it is striking that the majority of PG QSOs show stronger $[\text{O III}]$ emission than the highly polarized Type 1 2MASS objects for a given near-IR luminosity.

A proper comparison of the $[\text{O III}]$ emission between the near-IR and optically-selected samples awaits measurements for a larger sample of Type 1 2MASS objects, and the small number of objects presented here is strongly biased toward those showing high optical polarization. With these qualifications in mind, it appears that 2MASS is adept at finding red QSOs that, although exhibiting broad permitted emission lines in their total flux spectra, are underluminous in $[\text{O III}]$. A possible explanation for a link between the adopted red near-IR color selection and weak $[\text{O III}]$ strength may be that 2MASS finds AGN with a larger dust covering factor than is typical for optically-selected QSOs. Boroson & Meyers (1992) suggest a similar situation for the low-ionization broad absorption-line QSOs (BALQSOs) within the sample of infrared-selected AGN discovered by the *Infrared Astronomical Satellite* (IRAS; Low et al. 1988).

At the same time, there is no evidence from the objects of intermediate spectral type in this small sample that suggests a *fundamental* difference with UV-excess QSOs in terms of near-IR and $[\text{O III}]$ luminosity. For these AGN, it would appear that we have a relatively unobstructed view of the NLR that is powered by an continuum source indistinguishable from an optically-selected QSO if viewed from the line-emitting region.

4.1.2. Optical and Near-IR Continua

Although dramatic differences are not seen between the 2MASS and PG QSO samples in terms of $[\text{O III}]$ and near-IR luminosity, clear trends are observed in the optical spectral index (β_{OPT}). Figure 6 plots both the near-IR spectral

index (β_{IR} ; determined from the 2MASS JHK_s photometry) and the $B - K_s$ color index against β_{OPT} . The optical continuum is much redder for the 2MASS objects than for the comparison sample of PG QSOs with $z < 0.6$ measured by Neugebauer et al. (1987). The displacement of the 2MASS QSOs away from the PG QSOs in Figure 6 is generally consistent with that expected from reddening by dust, though for consistency with the PG data, β_{OPT} has not been corrected for the flux contribution made by the host galaxy. It is also the case that, for most of the 2MASS objects discussed here, a significant amount of the observed AGN flux is scattered into our line of sight. The scattered light does not appear to experience the same amount of reddening as the direct, unscattered light from the nucleus (see §4.2), and dust scattering typically results in a much bluer scattered light spectrum. Therefore, it is very difficult to ascribe a single reddening value to account for the spectral energy distribution throughout the entire optical/near-IR spectral region.

4.1.3. Balmer Decrement

Another reddening indicator is given by the $\text{H}\alpha/\text{H}\beta$ flux ratio. This quantity can be measured in 17 of the 21 objects observed. Generally, $\text{H}\alpha/\text{H}\beta$ is much larger than typically found for optically-selected QSOs, and in several objects it is measured to be >10 . It can be seen in Figure 7 that, at least for Type 1 and 1.5 QSOs, there is a trend between the Balmer decrement and the slope of optical continuum of the AGN. As expected from dust extinction, larger Balmer decrements tend to be observed for objects with redder optical continua.

For Figure 7, the estimated contributions from host galaxy starlight have been subtracted from the spectrum. The fluxes of the Balmer lines include both broad and narrow-line components, and $[\text{N II}]\lambda\lambda 6548, 6583$ has not been deblended from $\text{H}\alpha$. The $[\text{N II}]$ lines are only significant relative to $\text{H}\alpha$ for the Types 1.9 and 2 objects, and even reducing the measured $\text{H}\alpha$ flux by a factor of 2 to account for the blended forbidden lines still implies a large Balmer decrement for these QSOs.

Figure 7 also includes a rough reference point for comparison of the 2MASS QSOs with optically-selected QSOs. The star in the figure represents the median high frequency power-law fit to PG QSOs with $z < 0.6$ (Neugebauer et al. 1987) and $\text{H}\alpha/\text{H}\beta$ ($=3.7$) measured from the QSO template spectrum constructed from the *Sloan Digital Sky Survey* (SDSS; Vanden Berk et al. 2001). Roughly half of the Type 1 2MASS QSOs and all of the Type 1.5-2 objects have much larger Balmer decrements than the adopted optically-selected composite QSO.

For each of the Type 1 and 1.5 objects that have their Balmer decrement measured from the $q' \times F_\lambda$ spectrum, $\text{H}\alpha/\text{H}\beta$ is smaller in polarized light than observed in the total flux spectrum (Table 3). However, a proper comparison between the polarized and total flux Balmer decrements requires that only the broad Balmer-line components be used to determine the decrement since the polarized flux spectra of the 2MASS QSOs are generally devoid of NLR features. The narrow-line contribution to $\text{H}\alpha$ and $\text{H}\beta$ is not significant for the Type 1 objects, but by definition, the Type 1.5 QSOs exhibit Balmer lines with distinct broad-line and narrow-line components. After de-

blending the components and subtracting an estimate of the $[\text{N II}]\lambda\lambda 6548, 6583$ flux from $F_{\text{H}\alpha}$, a broad-line Balmer decrement is derived. The resolution of the observations does not permit direct measurement of $[\text{N II}]$ and we have assumed that the forbidden-line flux equals that of narrow $\text{H}\alpha$, close to the average line ratio for AGN (see e.g., Veilleux & Osterbrock 1987). It is clear from this exercise that broad $\text{H}\alpha$ dominates the line flux in the five Type 1.5 QSOs that have measured Balmer decrements. The broad-line Balmer decrements are found to be roughly the same as those given in Table 3 for the total flux spectra, and therefore, the fact that the decrement is smaller in polarized light is not caused by the inclusion of narrow-line flux.

The smaller polarized Balmer decrements suggest that the scattered light may undergo less reddening than the total AGN light. In fact, since $F_{\text{H}\alpha}/F_{\text{H}\beta} < 4$ for several objects, either there is little reddening from the nucleus to the scatterers and from the scatterers to us, or the scattering efficiency is higher at shorter wavelengths. In the latter case, electron scattering would be ruled out.

4.2. Polarization Properties

Because all of the highly polarized 2MASS QSOs are included in this study, these objects are largely responsible for the correlations between the degree of polarization, near-IR luminosity, and $B - K_s$ found by Smith et al. (2002). That is, AGN with high near-IR luminosity and near-IR-to-optical flux ratios tend to be highly polarized. These trends are consistent with a model that consists of 1) unpolarized, reddened AGN light that is observed directly, 2) unpolarized starlight of the host galaxy, and 3) AGN light polarized by scattering into our line of sight. Smith et al. argue that the majority of Type 1 objects are not highly polarized because the unscattered nuclear light dominates any source of polarized light. From our analysis of selected objects, it appears clear that the Type 2 QSOs show little broadband polarization because of host galaxy dilution, despite the fact that their extremely red colors imply heavy extinction of nuclear light along our line of sight. It may also be that the obscuration is so pervasive in the Type 2 QSOs that the light from the scattering region is also obscured. The intermediate QSOs show the highest mean polarization. For these, Smith et al. (2002) suggest that our direct view of the nucleus is more heavily obscured than for a typical Type 1 2MASS QSO, so that AGN light scattering into our view is not swamped by direct nuclear light. The fact that the QSOs of higher intrinsic luminosity tend to be the highly polarized objects in the sample is a consequence of the ability of the luminous AGN to better illuminate scattering material.

4.2.1. Continuum Polarization

Starlight from the host galaxies of many 2MASS QSOs results in continuum polarization being substantially less than if the AGN light could be observed in isolation. The 6000–7000 Å polarizations for 14 QSOs after the subtraction of the best estimates for the diluting stellar continua are listed in Table 3. The observed polarizations of the remaining objects are also listed since these objects show no evidence of significant “contamination” by the host galaxy. Not all objects exhibit high polarization even after the stellar continuum is taken into account, but these

results support the assertion by Smith et al. (2002) that the distribution of polarization of the 2MASS sample is even more distinct from optically-selected samples than suggested from raw broadband polarimetry. A striking example of the effects of dilution is given by 2M130005 (Figure 3 and Schmidt et al. 2002). Both the broadband measurement and the subsequent spectropolarimetry yield $P < 3\%$ in the R -band, but correction for the obvious late-type stellar spectrum implies an intrinsic polarization of the nuclear light of around 10%.

A wide range of continuum slopes are observed for the polarized flux and the host galaxy-subtracted total flux spectra. The power-law spectral indices for both F_λ and $q' \times F_\lambda$ are listed in Table 3. It can be seen in Figure 8 that for most 2MASS QSOs the polarized flux spectra are much bluer than observed for the optical AGN total flux, but $\beta_{q' \times F_\lambda}$ is still generally redder than the median optical continuum for the PG QSOs ($\beta_{\text{OPT}} \sim -1.6$; Figure 7). Two factors are most likely responsible for bluer polarized flux continua: the scattered light from the nuclear region experiences less reddening than the light directly seen from the AGN, and/or the scattering is more efficient in the blue than at longer wavelengths. The second effect, if applicable, rules out electron scattering and strongly hints that the scattering particles are dust grains. Although $\beta_{q' \times F_\lambda}$ tends to be bluer than β_{F_λ} , the polarized flux can be very red. Again, 2M130005 provides an extreme case of a red polarized continuum (Schmidt et al. 2002), and 2M170003 also shows $\beta_{q' \times F_\lambda} > 2$. The similarity of polarized and total flux spectral indices for each of these QSOs suggests that the light from the scattering regions is reddened by an amount comparable to the total flux spectrum.

Five objects have measured spectral indices for the polarized continuum that are redder than those for the total flux spectrum of the AGN. Each of these measurements, however, is much more uncertain than indicated by the formal error bars displayed in Figure 8. The error bars do not fold in the uncertainty in the fraction of host galaxy starlight. Of the five QSOs, polarizations $\lesssim 1.0\%$ are observed for 2M100121, 2M125807, and 2M222221, making measurement of the polarized continuum difficult. Inspection of Figure 2 for 2M222221 does show that the polarized continuum between $\text{H}\beta$ and $\text{H}\alpha$ is redder than F_λ over the same wavelength range. Low polarization also hampers measurement of $\beta_{q' \times F_\lambda}$ for 2M105144, 2M132917, and 2M222554; objects showing blue polarized continua relative to their total flux spectra. 2M010835 and 2M171559 are the two remaining QSOs measured to have redder polarized continua, but the value of β_{F_λ} is highly dependent on the choice of AGN-to-host galaxy flux ratio. This is true for all objects with large fractions of starlight in their spectra, mostly the Type 1.8–2 QSOs. The fraction of host galaxy flux is highly uncertain for both 2M010835 and 2M171559 simply because of the weak continua observed for these QSOs.

4.2.2. Broad-Line Polarization and Hidden BLRs

The vast majority of 2MASS QSOs included in this study exhibit broad Balmer lines in their polarized flux spectra. Some objects show polarization structure across the line profiles (see below), but in general the line polarizations are similar to that of the continuum in degree

and position angle. This fact excludes synchrotron radiation in general as the source of polarization. There are possibly only five QSOs in the sample that do not have polarized broad permitted lines. Three objects, 2M100121, 2M125807, and 2M222554 are very weakly polarized, making the identification of spectral features difficult. The only Type 1 object that shows no evidence for polarized emission lines is 2M125807, and it has the lowest polarization of the eight objects observed. The case of 2M222202 is detailed in §3.3.6 and the available data do not allow an unambiguous identification of weak polarized $H\beta$ despite the high S/N polarized flux spectrum (Figures 2 and 4). For this reason, a highly polarized synchrotron continuum cannot be ruled out for 2M222202, but observations at three epochs spanning 2.5 yr have not shown the object to be variable. Emission from $H\beta$ also cannot be identified in the much lower S/N polarized flux spectrum of the optically faint QSO 2M171559.

Given the resolution and S/N of the spectropolarimetry, the polarized and total flux line widths of the Balmer lines are roughly equivalent for the Type 1–1.5 QSOs. This implies that the scattering material is illuminated by an emission-line spectrum that is not much different from the BLR spectrum observed in our line of sight. The Balmer line widths tabulated in Table 2 identify four Type 1.5 QSOs with seemingly broader Balmer lines in polarized flux than in total flux. The decreased FWHM of the Balmer lines measured in the total flux spectrum of 2M134915, 2M165939, and 2M222221 is caused by the prominent narrow-line component largely absent from the polarized line profile. A Balmer emission-line component as broad as the polarized emission features can be seen in the total flux spectrum for all three of these objects. In the case of 2M222202, $H\beta$ is tentatively measured to be very broad (FWHM $\sim 17,000 \text{ km s}^{-1}$), although the emission feature is very weak and may even be misidentified.

The Type 1.8–2 objects with measured Balmer-line widths for both total and polarized flux spectra are represented by 2M010835, 2M105144, and 2M130005. The latter two objects were originally added to the sample to search for hidden BLRs, and both, in fact, exhibit very broad $H\alpha$ lines in polarized flux. This broad-line component can also be seen in the high S/N total flux spectrum of 2M105144 (Figure 3) and has been noted in 2M130005 by Schmidt et al. (2002).

2M130005 presents a dramatic example of a situation where emission from high-velocity clouds in the BLR is scattered into our line of sight. Though the broad $H\alpha$ line is extremely difficult to discern in the total flux spectrum, it appears as a very prominent, broad feature in polarized flux (Schmidt et al. 2002). Of course, hidden BLRs have been found in many Seyfert 2s (Antonucci & Miller 1985; Miller & Goodrich 1990; Tran 1995), NLRGs (Ogle et al. 1997; Cohen et al. 1999), and HIGs (Hines & Wills 1993; Hines et al. 1995; Young et al. 1996; Goodrich et al. 1996), and these discoveries have greatly promoted the idea that orientation of the nuclear region to the line of sight largely determines the “type” of AGN that we perceive. The results from 2M105144 and 2M130005 suggest that near-IR-selected AGN will also provide a number of similar objects; many with the intrinsic luminosity of a QSO.

Large polarized Balmer decrements and/or red polarized continua are observed for 2M010607, 2M150113, 2M130005, 2M163700, and 2M170003, and this may imply that the scattering region, as well as the nucleus, is highly reddened along the line of sight, or that light from the nucleus is reddened before reaching the scatterers. It may be common for the scattering regions in 2MASS QSOs to be reddened either by the dust torus that obscures the direct view to the nucleus, or by dust in the body of the host galaxy. A practical consequence of significant extinction of the extended scattering regions for Type 2 objects is that hidden BLRs will be more difficult to uncover polarimetrically.

Several 2MASS QSOs show higher polarization at $H\alpha$ and/or $H\beta$ compared to the local continuum. Good examples are 2M130005 and 2M134915, and this property can be attributed to dilution of the polarized light by an unpolarized continuum. Because the flux of the emission lines is not as heavily diluted as the polarized continuum, the polarization rises with the line profile. The same effect is often seen in highly polarized Seyfert 2s and radio galaxies, but for many of these objects, careful subtraction of the stellar light still leaves the broad emission lines more highly polarized than the continuum (see e.g., Tran 1995; Cohen et al. 1999). Another unpolarized, featureless continuum (FC2) of unknown origin, is generally invoked to bring the intrinsic continuum polarization to parity with that of the BLR, avoiding the physically untenable situation of having nuclear light, originating from a very compact region, be less polarized than the light from a more extended region surrounding the continuum source. Within the S/N of the spectropolarimetry of this optically faint sample, division of $q' \times F_\lambda$ by the total flux spectra after subtraction of the estimated stellar continua yields polarization levels at $H\alpha$ and $H\beta$ consistent with the local continuum polarization. Therefore, the existence of FC2 in the 2MASS sample is not supported by the observations.

Beyond the effect of the host galaxy continuum on the polarization of the broad Balmer lines relative to the continuum polarization, four 2MASS QSOs exhibit variations in polarization across the Balmer-line profiles. 2M004118 and 2M151653 most clearly show changes in both P and θ at the positions of the BLR features (Figure 1 and Smith et al. 2000). In both cases, the blue wings of the lines are less polarized than the red wings, but inspection of Figure 1 reveals that the behavior of θ across $H\alpha$ is different for the two QSOs. For 2M132917 (Figure 1), deviations of P and θ from the level of the local continuum appear to be restricted to the line core of $H\alpha$. 2M222221 (Figure 2) also shows complex rotations of θ across $H\alpha$ and, in contrast to 2M004118 and 2M151653, diminished polarization in the line’s red wing.

The wavelength dependence of the polarization across the BLR emission features implies a degree of complexity for the BLR and/or scattering regions. It also implies that the scattering material is located quite close to the BLR for these 2MASS QSOs, since polarization structure is very difficult to explain if the BLR is unresolved from the vantage point of the scattering clouds. Spectropolarimetry of several other Type 1 AGN have shown similar features. Goodrich & Miller (1994) and Smith et al. (1997) have identified cases among Seyfert 1 nuclei (see also Martel

1997; Smith et al. 2002), and Cohen et al. (1999) have done the same from a small sample of broad-line radio galaxies (BLRGs; namely, 3C 227 and 3C 445). Apparently, the phenomenon is independent of the radio power of the AGN.

Cohen et al. (1999) suggest a scenario to explain the complex polarization position angle rotations observed in broad $H\alpha$ for 3C 445 using the assumption that the gas motion within the BLR is not chaotic. For instance, the BLR emission could be scattered off of the inner wall of a dusty torus that is coplanar with the orbiting BLR clouds. If the emission line is broadened by the orbital motion of the BLR gas, and not the thermal motion of the gas nor the motion of the scatterers, the position angle difference between the red- and blue-shifted line emission can be explained by the fact that the two line components illuminate the scattering material from different directions. Cohen et al. (1999) point out that such a scenario works over a restricted range of inclination angles. The BLR also needs to be viewed directly since broad lines are prominent in the total flux spectrum, but if the inclination of the dust torus is too high, the scattering region that gives rise to the wavelength dependence of θ across the line will be obscured by the torus. A similar scenario with narrower spectral features than 3C 445 could be applicable to 2M004118 and 2M222221, but the variety of wavelength dependences in P and θ precludes a single geometry in all Type 1 objects. For example, the Seyfert 1 Mrk 486 (Smith et al. 1997) also requires at least two polarized emission-line components to describe the polarization at $H\alpha$, but instead of being shifted in wavelength, the components have different widths.

4.2.3. *The Polarization of the NLR and the Location of the Scattering Material*

Emission from the NLR is observed to have low polarization in a wide variety of polarized AGN samples where scattering of nuclear light into our line of sight is thought to be the polarizing mechanism. This is interpreted as the result of the scattering material being located within, or just exterior to, the NLR. In this respect, the highly polarized 2MASS QSOs resemble for example, polarized Seyferts, BLRGs, and HIGs since they all show much reduced polarization in their prominent narrow emission lines. Close proximity of the scatterers to the nuclear region is also required for the QSOs that show polarization variations with wavelength across their broad emission-line profiles (§4.2.2). Besides giving an indication of the location of the scattering regions, the differentiation of the NLR polarization from the continuum and BLR validates the assumption made in §2 that Galactic ISP is not the source of polarized flux for the sample.

Polarized $[O\ III]\lambda 5007$ is convincingly detected in six of the 2MASS QSOs: 2M010835, 2M091848, 2M130005, 2M134915, 2M222202, and 2M222221, plus 2M135852. The level of polarization for the NLR is $<3\%$ for all of these QSOs (last column of Table 3). All spectral classes are represented in the small number of objects showing polarized $[O\ III]\lambda 5007$. In general, the NLR shares a common polarization position angle with the continuum and BLR, although the polarization of the NLR in 2M222202 is deduced from the rotation in θ seen in the prominent nar-

row emission-lines. The level of polarization of the NLR is low enough that transmission through aligned dust grains within the body of the host galaxy cannot be ruled out as the polarizing mechanism, but the common polarization position angle of the NLR and the continuum observed in most objects suggests that the material scattering the continuum and BLR light also scatters and polarizes the inner NLR. 2M130005 provides evidence suggestive of the scattering material being located throughout the NLR (Schmidt et al. 2002). A polarization of $\sim 1.5\%$ is found for $[O\ III]\lambda 5007$, whereas the lower ionization $[S\ II]\lambda\lambda 6716, 6731$ lines are unpolarized. In addition, the relative strengths of narrow $H\alpha$ and $[N\ II]\lambda\lambda 6548, 6583$ are noticeably different in polarized light *vs.* total flux, with $H\alpha$ being stronger the polarized light. These observations are consistent with the regions producing the $[O\ III]$ and narrow $H\alpha$ lines being located closer to the nucleus, and with the scattering material being possibly intermixed with the unpolarized NLR gas. Similar evidence for such a stratified NLR is also seen in the HIG IRAS P09104+4109 (Hines et al. 1999; Tran, Cohen, & Villar-Martin 2000).

If the continuum is polarized by scattering in 2M222202 (§3.3.6), then the scatterers must be located closer to the nucleus than in the other 2MASS QSOs, since the polarized spectrum is nearly featureless. The scattering medium in this case may be electrons, given that the scatterers are likely to be intermixed with the BLR gas. Scattering by dust further out in the NLR may be responsible for the observed polarization in the rest of the sample. Dust would naturally explain the diminished Balmer decrements and blue continua of the polarized flux spectra, although electron scattering coupled with reduced reddening along the line of sight to the scattering region is also consistent with the observations. Ultraviolet spectropolarimetry may hold the key to identifying the scattering material in 2MASS QSOs since the shape of the spectrum of UV polarized flux has been used to identify dust as the scatterers in other reddened AGN (e.g., Hines et al. 2001).

4.3. *Host Galaxies*

Direct imaging with *HST* of 29 2MASS QSOs by Marble et al. (2003) shows that the sample exhibits a large range of AGN-to-host galaxy flux ratios. In addition, Marble et al. (2003) find that a wide variety of host galaxy morphologies and luminosities are represented, and that no clear differences are seen between the 2MASS QSO hosts and the galaxies hosting UV-excess QSOs. Although there is little overlap between the samples, the spectropolarimetry also finds objects that show little or no evidence for a significant contribution to their spectra from starlight, as well as objects where the host galaxy dominates the observed continuum. Type 1.8–2 QSOs generally show the largest host galaxy-to-total flux ratios in this sample, while stellar absorption features cannot be definitively identified for most of the eight Type 1 objects. These results are consistent with the suggestion by Smith et al. (2002) that, unlike optically-selected QSO samples, dilution of the polarized flux by starlight has a major effect on the observed distribution of broadband polarization in the 2MASS QSO sample (see §4.2.1).

5. CONCLUSIONS AND SUMMARY

Spectropolarimetry of 21 highly polarized and narrow-line QSOs discovered by 2MASS reveals several important aspects of this near-IR color-selected sample:

1. The observations are consistent with scattering of nuclear continuum and emission from the BLR by dust or electrons located exterior to the BLR as the polarizing mechanism. In general, the low polarization of the NLR implies that the scatterers cannot be situated much further from the ionizing continuum source than the extent of the NLR. The close proximity of the scattering material to the BLR in some objects is also indicated by the observation of wavelength-dependent polarization across their broad emission-line profiles. For one object, 2M222202, the scatterers must be located very close to the nucleus because the broad emission lines are essentially unpolarized.

2. Nearly all of the polarized 2MASS QSOs have broad Balmer emission lines detected in their polarized flux spectra.

3. In addition to displaying a wide array of AGN spectral types, the 2MASS QSOs exhibit a huge range of optical continuum slopes and Balmer decrements. These properties are consistent with various amounts of reddening and extinction of AGN light for these objects. In general, the polarized flux continua are bluer than the total flux spectra (i.e., P increases to the blue), and the broad-line Balmer decrement is smaller in the polarized light. This trend can be explained if the scattering efficiency increases with decreasing wavelength (small dust grain scattering), or if the particles are electrons and the scattered light experiences less reddening than the direct light from the nucleus. Although the polarized flux spectrum tends to be bluer than the total flux spectrum for these QSOs, the polarized continuum can be extremely red and large Balmer decrements can be measured for the polarized flux spectrum. For several objects, these properties indicate that there is a significant amount of reddening of the scattering regions situated around the nucleus.

4. The 2MASS sample includes a few objects with hidden BLRs. Spectropolarimetry of the Type 2 QSO 2M130005 reveals an extremely broad $H\alpha$ emission line in polarized flux (Schmidt et al. 2002). A similarly broad feature is also detected in both the polarized and total flux spectra of 2M105144.

5. At optical wavelengths, $\gtrsim 50\%$ of the observed continuum for many objects is from stars in the host galaxy. The largest host galaxy contributions to the optical flux are generally found for the Type 1.8–2 QSOs. This result is consistent with the finding of Marble et al. (2003) from *HST* imaging, that the fraction of host galaxy-to-AGN light is generally larger for Type 1.8–2 objects than for Type 1 and 1.5 QSOs, and implies that the nuclear regions of Type 1.8–2 2MASS QSOs are typically more highly obscured in our line of sight. The spectropolarimetry also supports the inference made by Smith et al. (2002) that the low level of broadband polarization observed for Type 1.8–2 QSOs is primarily due to a large amount of unpolarized light included in the observation aperture. In particular, correction for the host galaxy starlight yields intrinsic optical polarizations of the nuclear continuum for some Type 1.8–2 QSOs of $\sim 10\text{--}20\%$.

6. The sample of eight Type 1 2MASS QSOs observed

have $[\text{O III}]\lambda 5007$ luminosities systematically lower than PG QSOs of similar M_{K_s} . Since the sample is biased toward highly polarized objects, this may not be a property of the 2MASS QSOs as a whole. However, at least for the selected QSOs, this finding suggests that dust obscuration extends over a larger solid angle than is typically inferred to account for the relative numbers of optical spectral types in simple unification schemes (e.g., Antonucci 1993). No difference in $[\text{O III}]$ luminosity is seen between presumably more heavily obscured Type 1.5–1.9 2MASS QSOs and unobscured optically-selected QSOs.

It appears that the same basic model of an AGN surrounded by a dusty torus, with scattering material located above and below the toroidal plane, can be applied to Seyfert 1 and 2 nuclei, narrow- and broad-line radio galaxies, HIGs, and now a large sample of red AGN discovered by 2MASS. Upon close examination, the 2MASS objects do not appear to differ systematically from previous optically-selected AGN in a variety of fundamental parameters. The primary difference seems to be the amount of extinction along our line of sight to the nucleus. Optical spectropolarimetry and $[\text{O III}]$ luminosities suggest that the obscuring material does not cover all of the sky as seen by the central engine, and that many 2MASS QSOs would appear as typical UV/optical QSOs if viewed from a different perspective.

In retrospect, it may not be surprising that many AGN are obscured to some degree from our direct view, since the nuclei are often hosted by galaxies that contain large amounts of dust. This situation was foreseen in Seyfert galaxies by Rowan-Robinson (1977), but the magnitude of the nuclear obscuration was not appreciated until the first IR surveys for AGN. An exciting and challenging aspect of the new near-IR sample is that it represents a large, possibly dominant, low-redshift AGN population (Cutri et al. 2001). It is clear from even the small number of objects observed in this study that the new search techniques are exploring larger ranges of inclination angle and obscuration of the active nucleus and its immediate environment than have been probed by traditional surveys.

While the 2MASS QSOs so far identified add to our understanding of AGN in the local universe, it is likely that more highly obscured objects are excluded by the selection criteria. At sufficiently high column depths, the J -band flux from the nucleus will fall below the 2MASS sensitivity limit or below that of the host galaxy, making color selection inefficient. Surveys at longer wavelengths would alleviate this problem. The *Space Infrared Telescope Facility* (*SIRTF*) has the potential to uncover many more obscured AGN, but its coverage of the sky will be limited.

We thank the National Aeronautics and Space Administration (NASA) and the Jet Propulsion Laboratory (JPL) for support through *SIRTF*/MIPS and Science Working Group contracts 960785 and 959969 to The University of Arizona. Polarimetric instrumentation at Steward Observatory is maintained, in part, through support by National Science Foundation (NSF) grants AST 97–30792 and AST 98–03072. We also thank an anonymous referee for suggestions that improved the manuscript. This publication makes use of data products from the Two-Micron All Sky Survey, which is a joint project of the University of Mas-

sachusetts and the Infrared Processing and Analysis Center/California Institute of Technology, funded by NASA

and the NSF.

REFERENCES

- Antonucci, R. 1993, *ARA&A*, 31, 473
 Antonucci, R. R. J., & Miller, J. S. 1985, *ApJ*, 297, 621
 Baker, J. C. 1997, *MNRAS*, 286, 23
 Boroson, T. A., & Green, R. F. 1992, *ApJS*, 80, 109
 Boroson, T. A., & Meyers, K. A. 1992, *ApJ*, 397, 442
 Cohen, M. H., Ogle, P. M., Tran, H. D., Goodrich, R. W., & Miller, J. S. 1999, *AJ*, 118, 1963
 Condon, J. J., Cotton, W. D., Greisen, E. W., Yin, Q. F., Perley, R. A., Taylor, G. B., & Broderick, J. J. 1998, *AJ*, 115, 1693
 Cutri, R. M., Nelson, B. O., Kirkpatrick, J. D., Huchra, J. P., & Smith, P. S. 2001, in *ASP Conf. Ser. 232, The New Era of Wide Field Astronomy*, ed. R. G. Clowes, A. J. Adamson, & G. E. Bromage (San Francisco: ASP), 78
 Goodrich, R. W. 1995, *ApJ*, 440, 141
 Goodrich, R. W., & Miller, J. S. 1994, *ApJ*, 434, 82
 Goodrich, R. W., Miller, J. S., Martel, A., Cohen, M. H., Tran, H. D., Ogle, P. M., & Vermeulen, R. C. 1996, *ApJ*, 456, L12
 Hes, R., Barthel, P. D., & Fosbury, R. A. E. 1993, *Nature*, 362, 326
 Hines, D. C., Schmidt, G. D., Gordon, K. D., Smith, P. S., Wills, B. J., Allen, R. G., & Sitko, M. L. 2001, *ApJ*, 563, 512
 Hines, D. C., Schmidt, G. D., Smith, P. S., Cutri, R. M., & Low, F. J. 1995, *ApJ*, 450, L1
 Hines, D. C., Schmidt, G. D., Wills, B. J., Smith, P. S., & Sowinski, L. G. 1999, *ApJ*, 512, 145
 Hines, D. C., & Wills, B. J. 1993, *ApJ*, 415, 82
 Ho, L. C., Filippenko, A. V., & Sargent, W. L. W. 1997, *ApJ*, 487, 568
 Jackson, N., & Browne, I. W. A. 1990, *Nature*, 343, 43
 Kennicutt, R. C. 1992, *ApJ*, 388, 310
 Low, F. J., Huchra, J. P., Kleinmann, S. G., & Cutri, R. M. 1988, *ApJ*, 327, L41
 Marble, A. R., Hines, D. C., Schmidt, G. D., Smith, P. S., Surace, J. A., Armus, L., Cutri, R. M., & Nelson, B. O. 2003, *ApJ*, in press
 Martel, A. R. 1997, *PASP*, 109, 630
 Martel, A. R. 1998, *ApJ*, 508, 657
 Massey, P., Strobel, K., Barnes, J. V., & Anderson, E. 1988, *ApJ*, 328, 315
 Miller, J. S., & Goodrich, R. W. 1990, *ApJ*, 355, 456
 Neugebauer, G., Green, R. F., Matthews, K., Schmidt, M., Soifer, B. T., & Bennett, J. 1987, *ApJS*, 63, 615
 Norman, C., et al. 2002, *ApJ*, 571, 218
 Ogle, P. M., Cohen, M. H., Miller, J. S., Tran, H. D., Fosbury, R. A. E., & Goodrich, R. W. 1997, *ApJ*, 482, L37
 Rowan-Robinson, M. 1977, *ApJ*, 213, 635
 Schmidt, G. D., Elston, R., & Lupie, O. L. 1992, *AJ*, 104, 1563
 Schmidt, G. D., Stockman, H. S., & Smith, P. S. 1992, *ApJ*, 398, L57
 Schmidt, G. D., Smith, P. S., Foltz, C. B., & Hines, D. C. 2002, *ApJ*, 587, L99
 Schmidt, M., & Green, R. F. 1983, *ApJ*, 269, 352
 Serkowski, K., Mathewson, D. S., & Ford, V. L. 1975, *ApJ*, 196, 261
 Skrutskie, M. F., et al. 1997, in *The Impact of Large Scale Near-IR Surveys*, F. Garzon et al. eds., p. 25
 Smith, J. E., Young, S., Robinson, A., Corbett, E. A., Giannuzzo, M. E., Axon, D. J., & Hough, J. H. 2002, *MNRAS*, 335, 773
 Smith, P. S., Schmidt, G. D., Allen, R. G., & Angel, J. R. P. 1995, *ApJ*, 444, 146
 Smith, P. S., Schmidt, G. D., Allen, R. G., & Hines, D. C. 1997, *ApJ*, 488, 202
 Smith, P. S., Schmidt, G. D., Hines, D. C., Cutri, R. M., Nelson, B. O. 2000, *ApJ*, 545, L19
 Smith, P. S., Schmidt, G. D., Hines, D. C., Cutri, R. M., Nelson, B. O. 2002, *ApJ*, 569, 23
 Tran, H. D. 1995, *ApJ*, 440, 597
 Tran, H. D., Cohen, M. H., & Goodrich, R. W. 1995, *AJ*, 110, 2597
 Tran, H. D., Cohen, M. H., & Villar-Martin, M. 2000, *AJ*, 120, 562
 Tran, H. D., Miller, J. S., & Kay, L. E. 1992, *ApJ*, 397, 492
 Veilleux, S., & Osterbrock, D. E. 1987, *ApJS*, 63, 295
 Vanden Berk, D. E., et al. 2001, *AJ*, 122, 549
 Wardle, J. F. C., & Kronberg, P. P. 1974, *ApJ*, 194, 249
 Wilkes, B. J., Schmidt, G. D., Cutri, R. M., Ghosh, H., Hines, D. C., Nelson, B., & Smith, P. S. 2001, *ApJ*, 564, L65
 Wills, B. J., Netzer, H., & Wills, D. 1985, *ApJ*, 288, 94
 Wills, B. J., Wills, D., Evans II, N. J., Thompson, K. L., Berger, M., & Sitko, M. L. 1992, *ApJ*, 400, 96
 Young, S., Hough, J. H., Efstathiou, A., Wills, B. J., Bailey, J. A., Ward, M. J., & Axon, D. J. 1996b, *MNRAS*, 281, 1206

TABLE 1
OBJECTS AND OBSERVATIONS

Object (2MASS J)	z	Type	$M_{K_s}^a$	K_s^b	$B - K_s^b$	UT Date	Tel.	Slit Width ($''$)	Exp. (s)	P^c (%)	θ^c ($^\circ$)
004118.7+281640	0.194	1	-27.29	12.50	3.40	1999 Oct 14 2002 Jul 6 ave.	Bok MMT	3.0 1.1	7200 1920 9120	2.18 ± 0.02 2.28 ± 0.02 2.23 ± 0.01	97.9 ± 0.3 95.2 ± 0.3 96.9 ± 0.2
010607.7+260334	0.411	1	-27.58	14.61	>6.4	2000 Jan 9, 10	Bok	2.0,3.0	19200	7.84 ± 0.14	118.4 ± 0.5
010835.1+214818	0.285	1.9	-27.64	13.46	6.54	1999 Oct 13, 15	Bok	2.0	22400	5.07 ± 0.11	118.9 ± 0.6
091848.6+211717	0.149	1.5	-26.65	12.55	5.95	2000 Jan 9, 10	Bok	3.0	24800	6.49 ± 0.02	153.4 ± 0.1
100121.1+215011	0.248	2	-25.79	14.68	5.52	2002 Feb 15	MMT	1.1	3840	0.73 ± 0.16	150.5 ± 6.0
105144.2+353930	0.158	1.9	-25.77	13.54	5.06	2002 Feb 15	MMT	1.5	3840	1.18 ± 0.11	30.8 ± 2.7
125807.4+232921	0.259	1	-27.09	13.45	3.85	2000 Jan 10	Bok	3.0	4800	1.00 ± 0.03	107.7 ± 1.0
130005.3+163214 ^d	0.080	2	-25.84	11.86	5.24	2001 Apr 1 2002 Jan 5 2002 Jul 4, 5 ave.	MMT Bok MMT	1.1 3.0 1.1	3840 2400 8640 14880	2.58 ± 0.03 1.81 ± 0.77 2.51 ± 0.01 2.76 ± 0.01	50.8 ± 0.3 46.5 ± 1.2 43.7 ± 0.2 45.3 ± 0.1
132917.5+121340	0.203	1	-25.78	14.12	4.58	2001 Mar 31	MMT	1.1	3840	1.37 ± 0.05	13.8 ± 1.0
134915.2+220032	0.062	1.5	-24.87	12.24	3.27	2000 May 7 2001 Mar 30 ave.	Bok MMT	3.0 1.5	9600 8640 18240	1.84 ± 0.03 1.64 ± 0.03 1.78 ± 0.02	108.2 ± 0.5 104.0 ± 0.5 106.9 ± 0.3
135852.5+295413 ^e	0.113	1	-25.58	12.85	4.15	2000 May 7	Bok	3.0	12800	4.59 ± 0.02	23.0 ± 0.1
150113.1+232908	0.258	1	-27.24	13.46	5.84	2001 Mar 30, Apr 1	MMT	1.5,1.1	12480	3.40 ± 0.04	156.0 ± 0.3
151653.2+190048 ^f	0.190	1	-28.35	11.41	4.39	2000 May 9	Bok	3.0	6720	9.27 ± 0.01	106.5 ± 0.1
163700.2+222114	0.211	1.5	-26.44	13.59	5.41	2002 Jul 5	MMT	1.1	7200	2.49 ± 0.04	116.4 ± 0.4
165939.7+183436 ^g	0.170	1.5	-26.59	12.91	5.29	1999 Oct 13, 14, 15 2001 Mar 31 ave.	Bok MMT	3.0,2.0 1.1	9600 960 10560	5.34 ± 0.06 5.44 ± 0.09 5.33 ± 0.03	158.4 ± 0.3 160.0 ± 0.5 158.8 ± 0.2
170003.0+211823	0.596	1.5	-28.30	14.88	7.21	2001 Mar 31 2002 Jul 4 ave.	MMT MMT	1.1 1.1	5760 7200 12960	10.96 ± 0.15 11.10 ± 0.08 11.06 ± 0.04	108.4 ± 0.4 108.4 ± 0.2 108.7 ± 0.1
171559.7+280717	0.524	1.8	-28.14	14.63	>6.4	2002 Feb 19 2002 Jul 6 ave.	MMT MMT	1.1 1.1	1920 7200 9120	3.62 ± 1.11 5.03 ± 0.18 5.16 ± 0.08	0.3 ± 8.8 1.4 ± 1.0 1.5 ± 0.4
222202.2+195231	0.366	1.5	-28.60	13.30	6.20	1999 Oct 13, 15 2002 Jan 6 2002 Jul 4 ave.	Bok Bok MMT	2.0 2.0,3.0 1.1	19200 5760 4800 29760	11.41 ± 0.11 12.51 ± 0.25 11.59 ± 0.03 11.04 ± 0.04	118.1 ± 0.3 116.9 ± 0.6 118.8 ± 0.1 118.8 ± 0.1
222221.1+195947	0.211	1.5	-27.10	12.92	4.58	1999 Oct 15 2002 Jul 8 ave.	Bok MMT	3.0 1.5	6400 1920 8320	1.15 ± 0.04 0.96 ± 0.03 1.02 ± 0.02	156.4 ± 0.9 165.2 ± 0.8 161.7 ± 0.6
222554.2+195837	0.147	2	-25.65	13.49	5.31	2002 Jul 5	MMT	1.1	7200	0.28 ± 0.03	0.7 ± 3.4
230307.2+254503	0.331	1	-26.70	14.50	6.21	1999 Oct 14, 16 2002 Jul 8 ave.	Bok MMT	2.0 1.1	22400 2400 24800	3.31 ± 0.09 4.66 ± 0.19 3.47 ± 0.04	137.3 ± 0.8 138.3 ± 1.2 138.2 ± 0.3

^aThe K-corrected absolute K_s magnitude is from Smith et al. (2002) and is based on 2MASS photometry. The listed values assume that $H_0 = 75 \text{ km s}^{-1} \text{ Mpc}^{-1}$, $q_0 = 0$, and $\Lambda = 0$.

^bData are from the 2MASS Point Source Catalog.

^cThe flux-weighted mean optical linear polarization in the 5000–8000 Å band (observed frame). The listed degree of linear polarization has not been corrected for statistical bias.

^dObservations reported in Schmidt et al. (2002).

^e2M135852 is not considered a member of the 2MASS sample of QSOs since $J - K_s < 2$.

^fObservations reported in Smith et al. (2000).

^gObservations obtained with the Bok Telescope reported in Smith et al. (2000).

TABLE 2
EMISSION-LINE PROPERTIES

Object (2MASS J)	EW _{Hβ} ^a (Å) $F_{\lambda}/q' \times F_{\lambda}$	EW _{Hα} ^b (Å) $F_{\lambda}/q' \times F_{\lambda}$	EW _[O III] (Å) $F_{\lambda}/q' \times F_{\lambda}$	FWHM _{Hβ} ^a (km s ⁻¹) $F_{\lambda}/q' \times F_{\lambda}$	FWHM _{Hα} ^b (km s ⁻¹) $F_{\lambda}/q' \times F_{\lambda}$	F _{Hβ} ^{a,c} $F_{\lambda}/q' \times F_{\lambda}$	F _{Hα} ^{b,c} $F_{\lambda}/q' \times F_{\lambda}$	F _[O III] ^c $F_{\lambda}/q' \times F_{\lambda}$	Log $L_{[O III]}$ ^d (erg s ⁻¹) $F_{\lambda}/q' \times F_{\lambda}$	Notes
Type 1:										
004118.7+281640	81/...	500/130:	8/...	2280/...	1960/3200:	8.07/...	29.5/0.16:	0.72/...	41.95/...	1,2
010607.7+260334	71/87	N/A	20/...	1740/1880	N/A	0.20/0.02	N/A	0.06/...	41.71/...	
125807.4+232921	25/...	145/...	.../...	2350/...	2010/...	1.09/...	4.30/...	.../...	.../...	
132917.5+121340	75/180	300/...	29/<15	3660/4610	3610/...	1.18/0.05	4.75/...	0.45/<0.01	41.79/<39.7	1
135852.5+295413	36/68	275/550	14/6	6720/6590	5440/5430	2.21/0.18	15.00/1.14	0.75/0.02	41.41/39.77	
150113.1+232908	32/85	225/890	8/<7	2530/3170	2540/2580	0.23/0.03	2.71/0.18	0.06/<0.01	41.19/<39.8	
151653.2+190048	87/92	645/440	16/...	4040/4840	3680/4100	18.47/1.95	110.00/6.35	3.36/...	42.60/...	1
230307.2+254503	49/40	80:/...	10/...	2300/1550	1800:/...	0.22/0.01	0.6:/...	0.04/...	41.33/...	3
Type 1.5:										
091848.6+211717	44/74	240/230	62/18	1980/2270	1790/1800	0.85/0.11	6.54/0.35	1.19/0.03	41.89/40.21	4
134915.2+220032	63/260	310/480	185/73	1900/4580	1800/2620	2.69/0.17	15.90/0.49	7.44/0.05	41.82/39.66	5
163700.2+222114	25/49	220/320	42/...	1270/1930	2910/3700	0.12/0.01	2.47/0.09	0.32/...	41.69/...	
165939.7+183436	45/117	240/500	112/...	4110/15700	4270/7430	1.02/0.14	6.27/0.49	2.48/...	42.34/...	5,6
170003.0+211823	123/90	N/A	64/...	2630/2980	N/A	0.35/0.03	N/A	0.19/...	42.74/...	6
222202.2+195231	206/70:	N/A	173/...	2040/17000:	N/A	1.22/0.06:	N/A	1.03/...	42.84/...	7
222221.1+195947	118/240	880/1110	65/25	4260/7910	3390/6860	8.35/0.17	46.80/0.57	4.49/0.02	42.84/40.37	1
Type 1.8–2:										
010835.1+214818	56/43	430/480:	360/120	870/1320	1730/3100:	0.27/0.01	2.21/0.16:	2.43/0.04	42.91/41.10	3,5
100121.1+215011	7/...	190/...	24/...	1090/...	1830/...	0.03/...	0.80/...	0.09/...	41.30/...	3,5
105144.2+353930	5/...	270:/...	97/...	930/...	2000:/9000:	0.04/...	2.09/0.10:	0.55/...	41.61/...	5,8
130005.3+163214	5/...	57/415	57/56	1210/...	2060/18400	0.18/<0.14	3.67/0.45	1.61/0.03	41.40/39.61	5
171559.7+280717	130/...	N/A	450:/...	1090/...	N/A	0.19/...	N/A	0.6:/...	43:/...	8
222554.2+195837	4/...	72/...	43/...	960/...	2190/...	0.08/...	1.06/...	0.58/...	41.56/...	4,5

^aThe Hβ equivalent width (EW_{Hβ}), line width (FWHM_{Hβ}), and flux (F_{Hβ}) include the contributions from both the narrow- and broad-line components.

^bMeasurements of EW_{Hα}, FWHM_{Hα}, and F_{Hα} include the contributions from [N II]λλ6548,6583 and both the narrow- and broad-line components of Hα.

^cEmission-line fluxes have units of 10⁻¹⁴ erg cm⁻² s⁻¹.

^dLogarithm of the [O III]λ5007 luminosity.

Note. — (1) Structure in q' and θ in the line profile of Hα. (2) Data corrected for Galactic ISP. (3) Hα located near the edge of the observed spectrum. (4) The terrestrial A-band O₂ absorption band affects the red wing of Hα + [N II]. (5) Hα includes significant [N II]λλ6548,6583. (6) The extreme blue portion of Hα or Hβ is affected by O₂ A-band absorption. (7) Identification of a polarized spectral feature with Hβ is uncertain. (8) The Hα + [N II] flux ([O III]λ5007 for 2M171559) is uncertain because the redshifted lines fall within the O₂ A-band absorption feature.

TABLE 3
CONTINUUM PROPERTIES, LINE RATIOS, AND POLARIZATIONS

Object (2MASS J)	$F_{\text{gal}}/F_{\text{Total}}^{\text{a}}$	P^{b} (%)	θ^{b} ($^{\circ}$)	β^{c} $F_{\lambda}/q' \times F_{\lambda}$	$F_{[\text{O III}]} / F_{\text{H}\beta}^{\text{d}}$ $F_{\lambda}/q' \times F_{\lambda}$	$F_{\text{H}\alpha} / F_{\text{H}\beta}^{\text{d}}$ $F_{\lambda}/q' \times F_{\lambda}$	$F_{\text{Fe II}} / F_{\text{H}\beta}^{\text{d}}$ $F_{\lambda}/q' \times F_{\lambda}$	$P_{\text{H}\beta}^{\text{e}}$ (%) line/cont	$P_{\text{H}\alpha}^{\text{e}}$ (%) line/cont	$P_{\text{NLR}}^{\text{f}}$ (%)
Type 1:										
004118.7+281640	...	2.35 \pm 0.02	96.3 \pm 0.2	-2.2/-1.9	0.1/ ...	3.7/ ...	1.4/ /2.3	0.5:/2.1	...
010607.7+260334	...	7.73 \pm 0.20	117.3 \pm 0.8	+1.3/+0.5	0.3/ ...	N/A	0.8/ ...	9.1/8.6	N/A	...
125807.4+232921	0.1: [†]	1.05 \pm 0.06	111.4 \pm 1.7	-2.2/-1.0:	... / ...	3.9/ ...	2.1/ /2:	... /3:	...
132917.5+121340	...	1.32 \pm 0.07	11.4 \pm 1.6	-0.5/-2.0:	0.4/<0.1	4.0/ ...	0.7/ ...	4.1/2:	... /3:	<1
135852.5+295413	0.57	9.10 \pm 0.07	23.4 \pm 0.2	+0.7/-0.9	0.3/0.1	6.8/6.1	0.2/ ...	8.5/12.8	7.6/7.9	2.4
150113.1+232908	0.59	8.25 \pm 0.14	157.0 \pm 0.5	+2.3/+0.0	0.3/<0.1	11.6/7.1	0.7/ ...	10.7/12.2	6.5/6.1	<3
151653.2+190048	...	9.24 \pm 0.02	107.0 \pm 0.1	-0.9/-2.1	0.2/ ...	6.0/3.3	1.1/1.0	10.6/10.7	5.8/7.5	...
230307.2+254503	...	2.93 \pm 0.05	138.8 \pm 0.5	+0.9/-0.3	0.2/ ...	3:/ ...	3.3/ ...	3.7/7.0	... /5.0	...
Type 1.5:										
091848.6+211717	0.37	10.01 \pm 0.07	153.3 \pm 0.2	+1.0/-0.6	1.4/0.2	7.7/3.3	1.1/1.4	12.4/12.7	5.4/8.0	2.1
134915.2+220032	0.47	2.62 \pm 0.04	108.0 \pm 0.4	+0.8/+0.0	2.8/0.3	5.9/2.9	0.8/ ...	6.2/4.7	3.1/3.7	<1
163700.2+222114	0.51	4.46 \pm 0.10	115.6 \pm 0.6	+2.0/+0.9	1.6/ ...	12.6/9.2	1.1/ ...	8.3/7.4	3.6/5.4	...
165939.7+183436	0.26	7.14 \pm 0.12	158.8 \pm 0.5	-0.3/-0.7	2.4/ ...	6.2/3.5	... / ...	14.0/8.6	7.8/7.6	...
170003.0+211823	...	11.40 \pm 0.05	107.9 \pm 0.1	+2.1/+2.0	0.5/ ...	N/A	0.4/ ...	8.0/12.4	N/A	...
222202.2+195231	...	10.40 \pm 0.05	118.9 \pm 0.1	+0.6/-1.0	0.8/ ...	N/A	0.3/ ...	8:/14.1	N/A	0.8
222221.1+195947	0.3: [†]	1.15 \pm 0.04	163.7 \pm 1.0	-1.8/-0.2:	0.5/0.1	5.6/3.4	0.2/ ...	2.0/2:	1.2/3:	<1
Type 1.8-2:										
010835.1+214818	0.8:	22: \pm 1:	120.0 \pm 1.2	-2.3/-0.6	9.1/3.5	8.2/15:	... / ...	4.1/24:	7:/40:	1.6
100121.1+215011	0.84	2.58 \pm 1.11	152.7 \pm 12.4	-0.7/+0.5:	3.3/ ...	31/ / /20:	... /30:	...
105144.2+353930	0.71	2.72 \pm 0.55	38.3 \pm 5.8	+2.4/+0.6:	15/ ...	57:/ / /20:	5:/10:	...
130005.3+163214	0.81	9.50 \pm 0.07	44.7 \pm 0.2	+3.6/+3.0	8.9/ ...	20/>3	... / /11.9	12.2/9.8	1.6
171559.7+280717	0.5: [†]	18.5: \pm 0.4:	2.4 \pm 0.7	-0.0/+0.8:	3:/ ...	N/A	... / /17:	N/A	...
222554.2+195837	0.80	1.00 \pm 0.24	7.2 \pm 6.8	+1.2/+0.4:	7.8/ ...	14/ / /7:	... /5:	...

^aThe adopted ratio of host galaxy starlight to total light at a rest frame wavelength of 5500 Å determined from observed stellar absorption features or from Marble et al. (2003) ([†]).

^bFlux-weighted linear polarization in the 6000–7000 Å band (observed frame). Values of P are corrected for dilution by unpolarized starlight from the host galaxy using the estimate given by $F_{\text{gal}}/F_{\text{Total}}$ in this table. The degree of polarization is not corrected for statistical bias.

^cThe continuum spectral slopes for the total flux (F_{λ}) and polarized flux ($q' \times F_{\lambda}$) spectra. Host galaxy starlight has been subtracted from F_{λ} before fitting a power law to the continuum.

^dThe H α and H β fluxes include the contributions from both the narrow- and broad-line components. In the case of H α , flux from [N II] $\lambda\lambda$ 6548,6583 is also included.

^eThe first entry in the column is the estimate of the emission-line polarization based on the measurements of the line flux in the total and polarized flux spectra (Table 2). The second entry is the continuum polarization at the wavelength of the line determined by the power-law fits to the total and polarized spectra (see text).

^fThe polarization of the emission from the NLR, based on measurements of [O III] λ 5007.

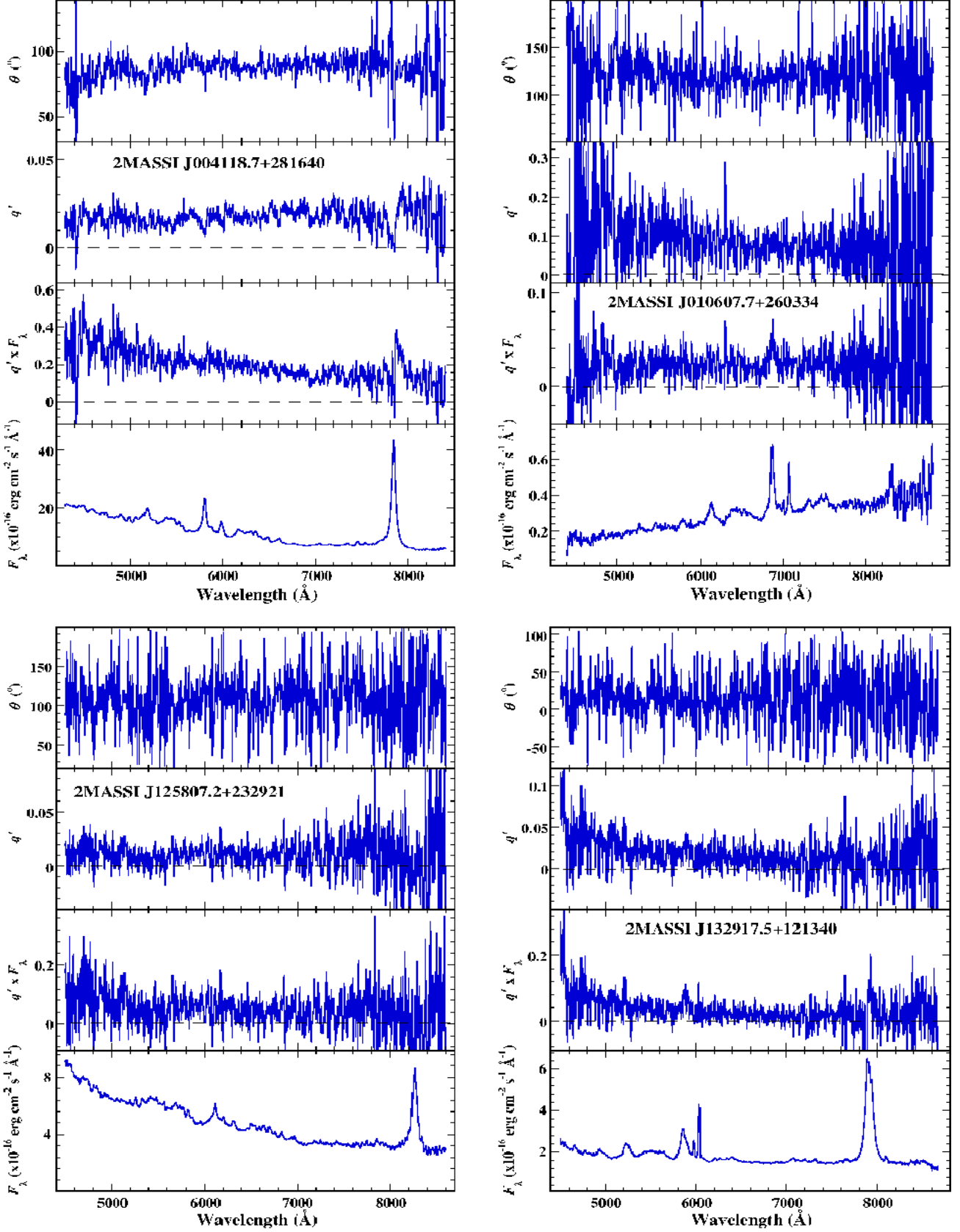


FIG. 1.— Spectropolarimetry of Type 1 2MASS QSOs. For each object the panels display (from bottom to top) the spectra of total flux density (F_{λ}), Stokes flux density ($q' \times F_{\lambda}$) for a frame aligned with the mean polarization position angle at 5000–8000 Å, rotated Stokes parameter (q'), and the equatorial polarization position angle (θ).

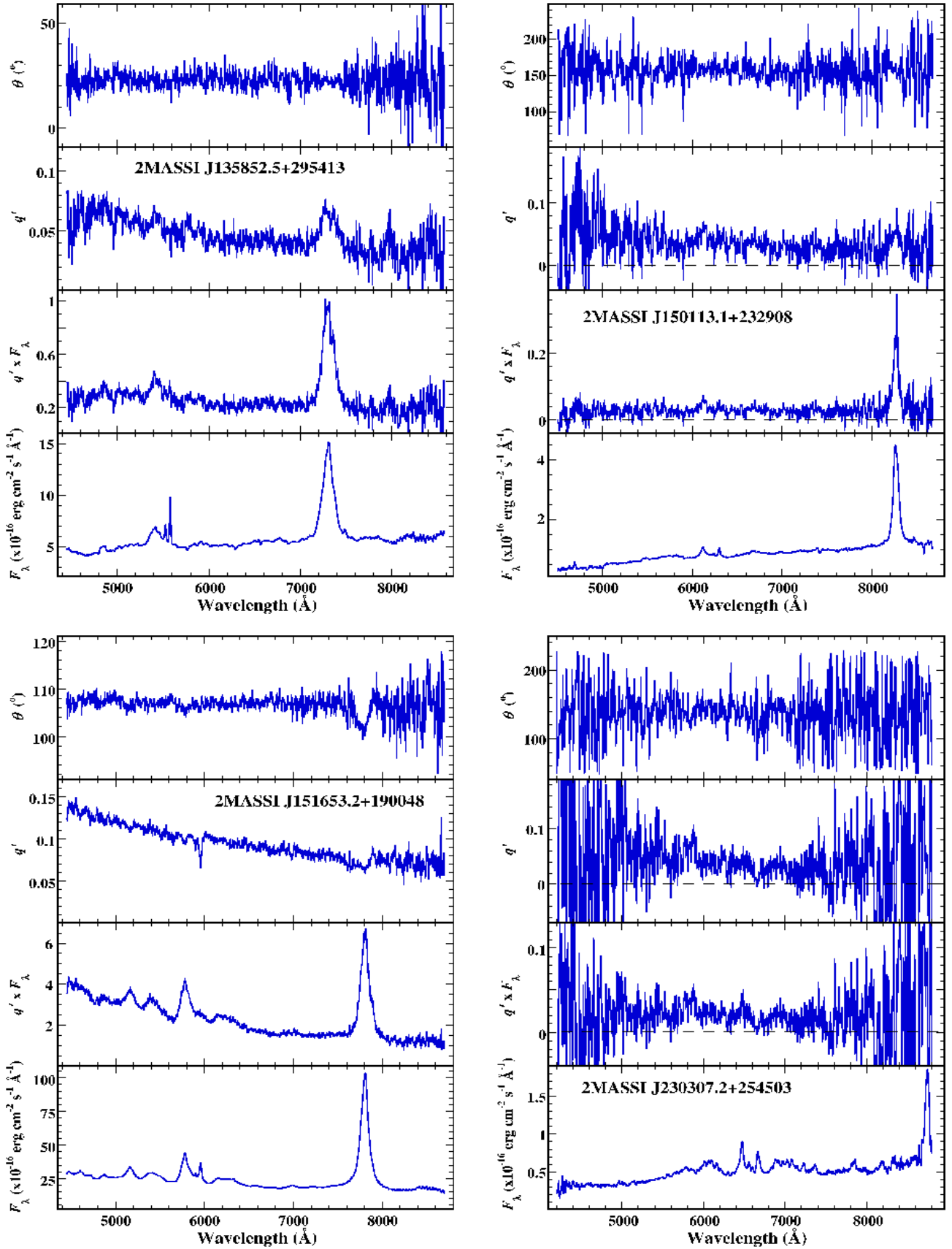


FIG. 1.— Continued.

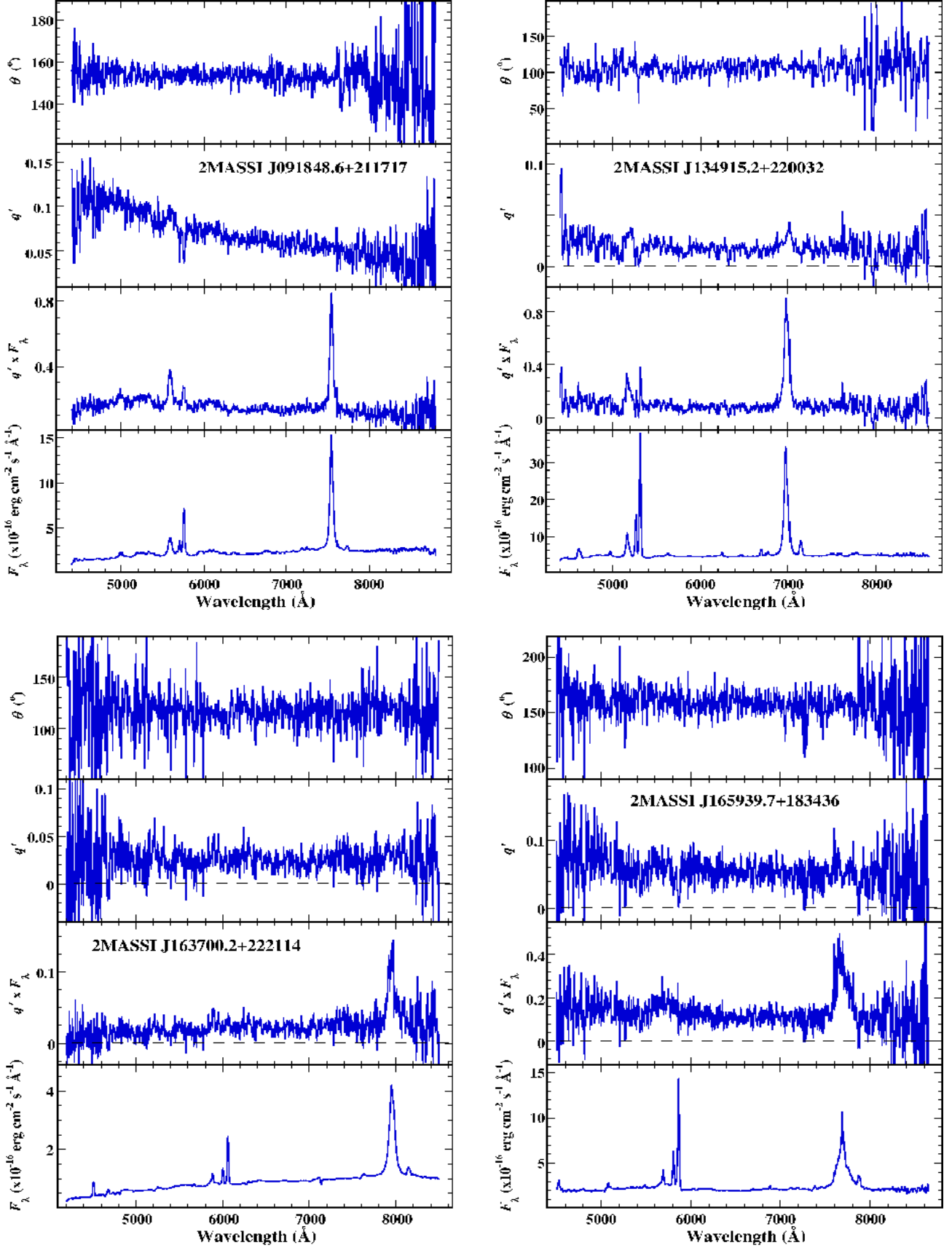


FIG. 2.— Spectropolarimetry of Type 1.5 2MASS QSOs. The data are displayed in the same format as in Figure 1.

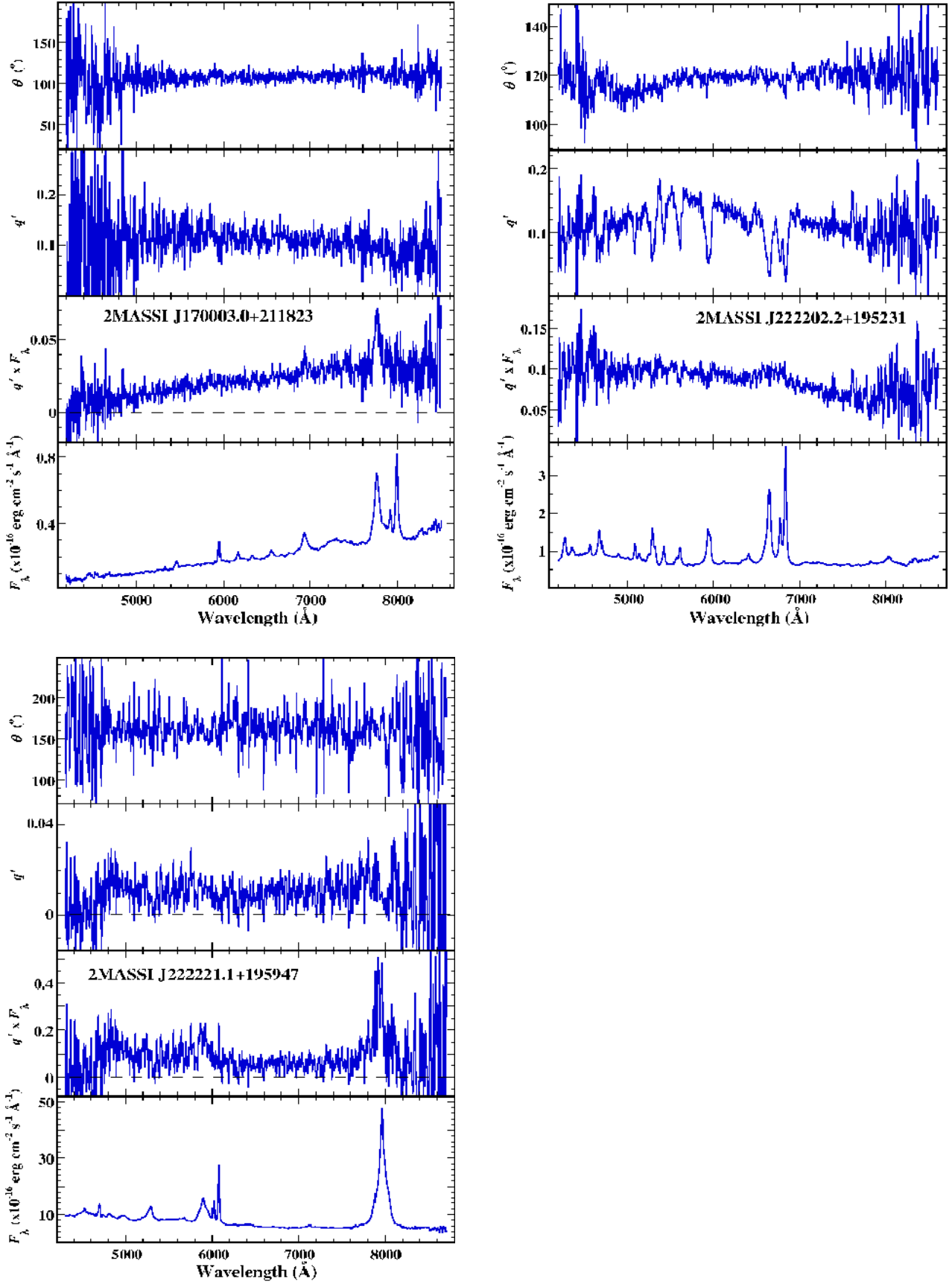


FIG. 2.— Continued.

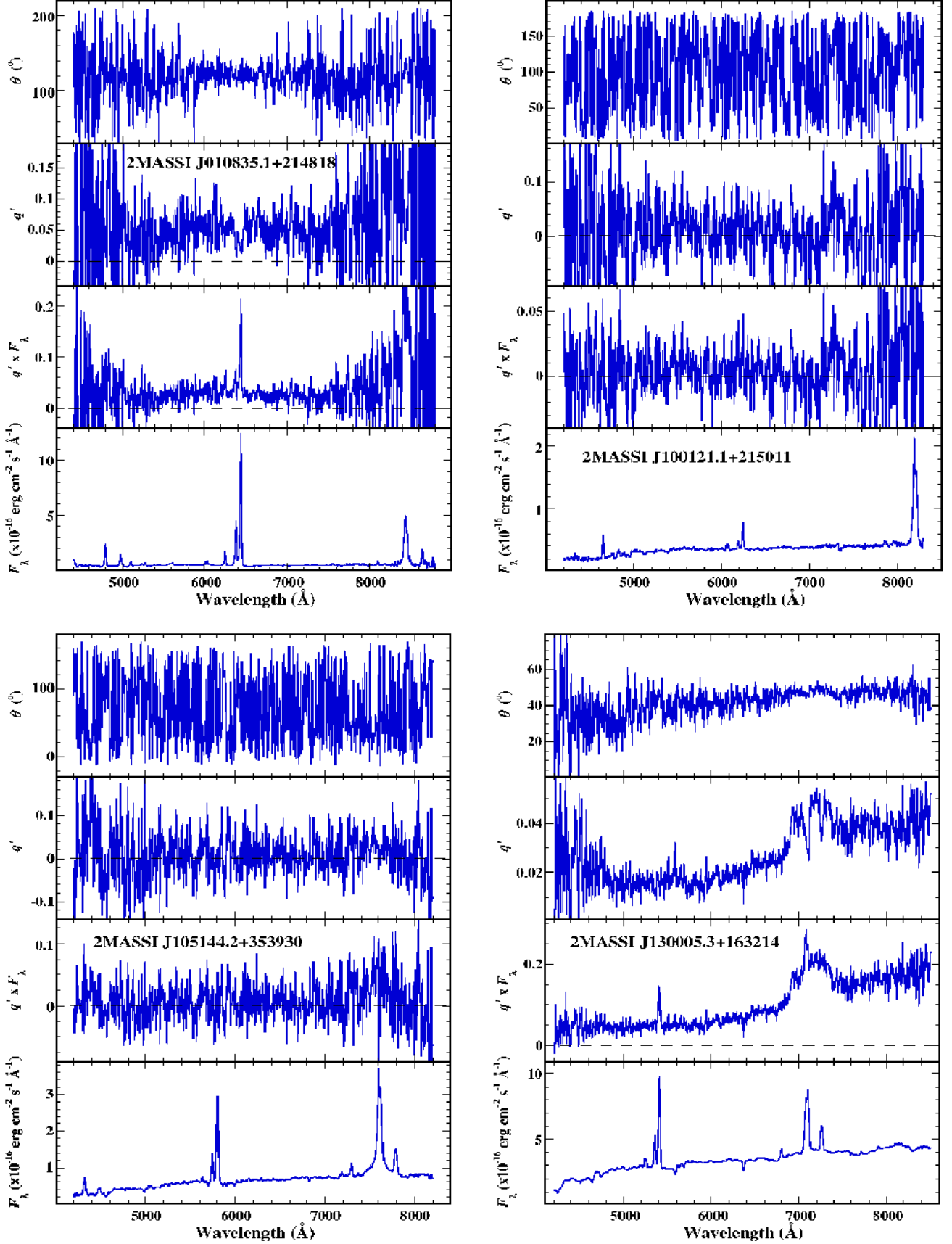


FIG. 3.— Spectropolarimetry 2MASS QSOs of Types 1.8, 1.9, and 2. The data are displayed in the same format as in Figure 1.

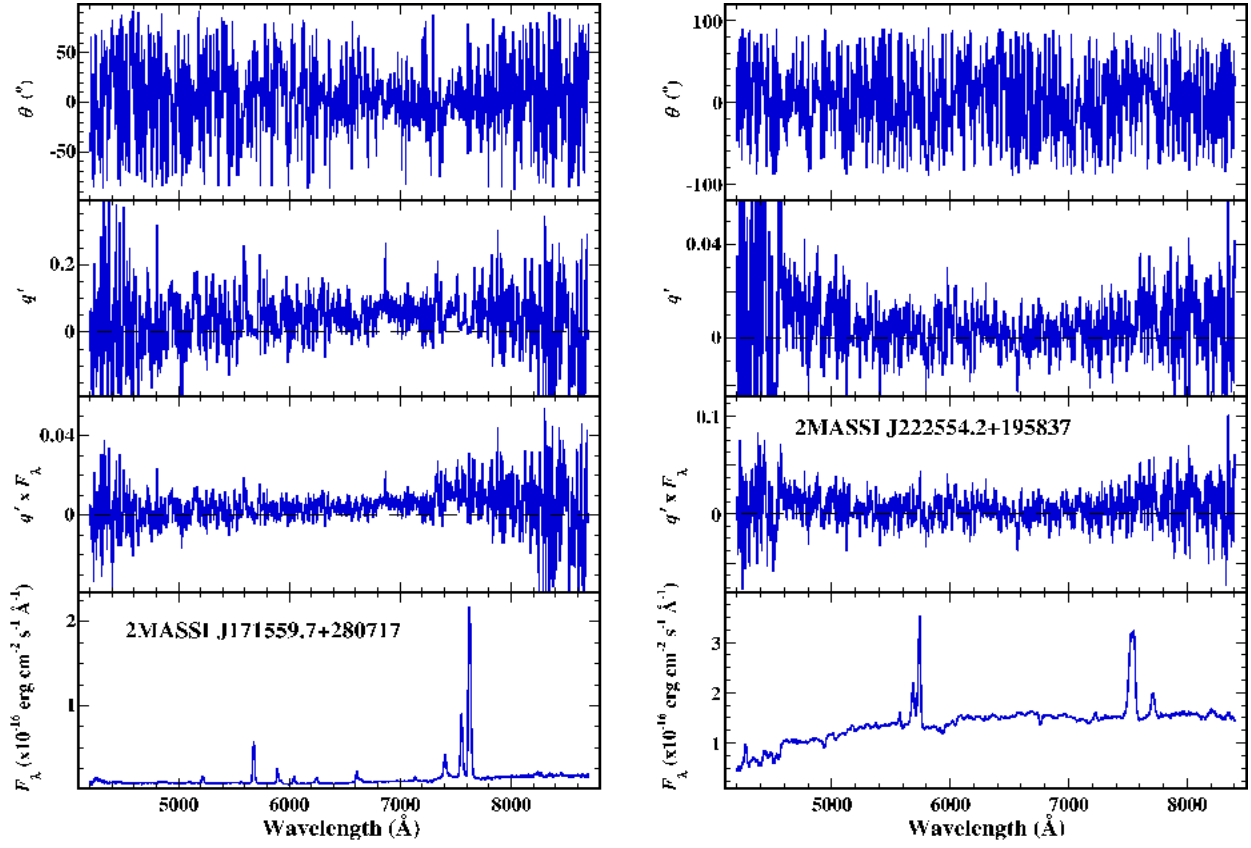


FIG. 3.— Continued.

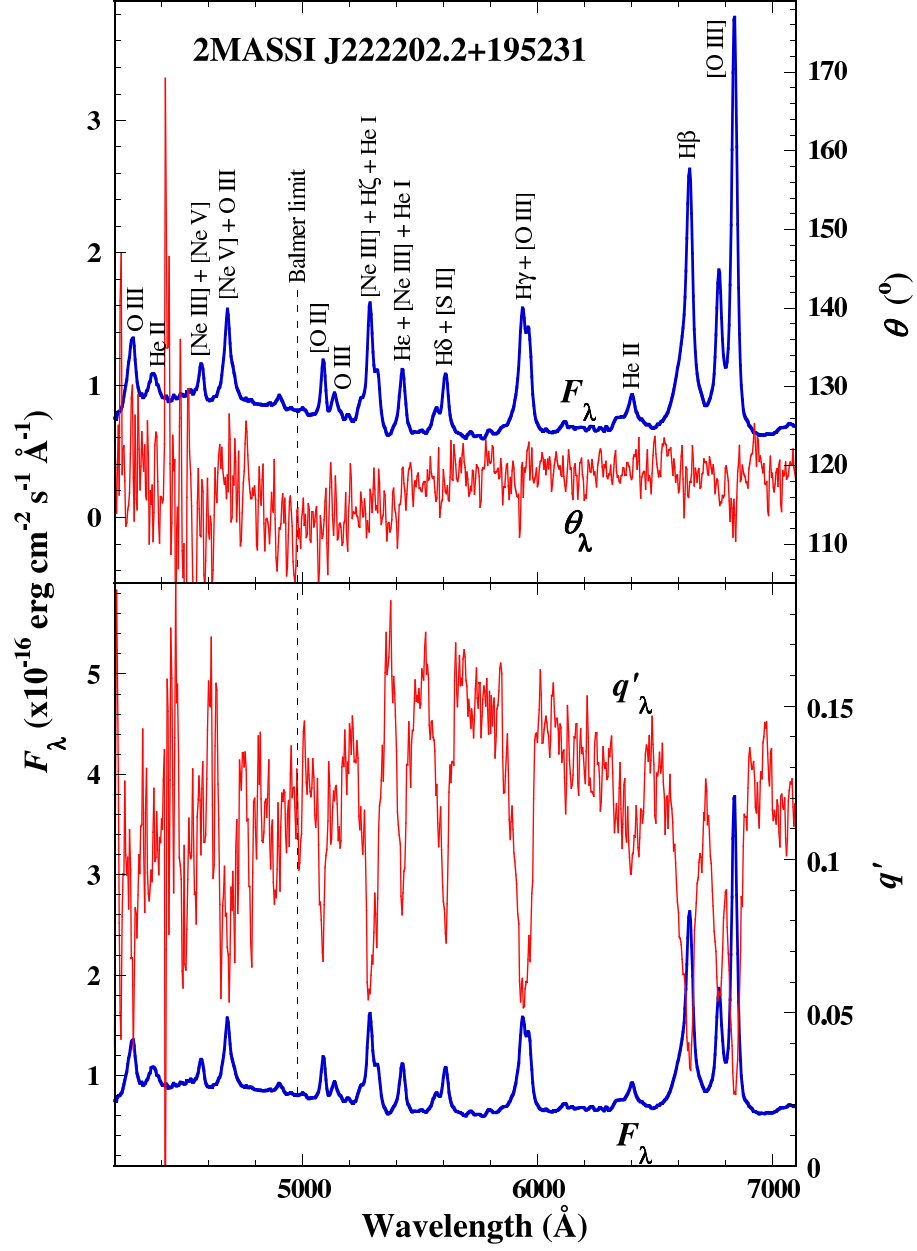


FIG. 4.— A detailed view of the flux spectrum and polarization of 2M222202. Major emission lines are identified for the total flux spectrum in the top panel which compares F_{λ} with the spectrum of the polarization position angle. The total flux spectrum is again displayed in the bottom panel for direct comparison with with the rotated Stokes parameter q' .

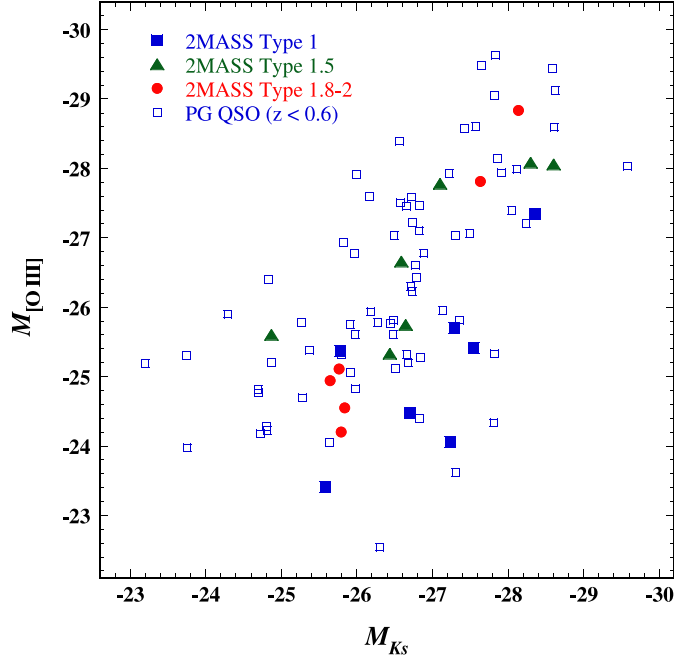


FIG. 5.— Luminosity of $[\text{O III}]\lambda 5007$ plotted against M_{K_s} for the 2MASS spectropolarimetry sample and PG QSOs with $z < 0.6$. The measure of $[\text{O III}]$ luminosity, $M_{[\text{O III}]}$, is adopted from Boroson & Green (1992) (see text). The near-IR luminosity of the PG QSOs is determined from the observations of Neugebauer et al. (1987) and assume $H_0 = 75 \text{ km s}^{-1} \text{ Mpc}^{-1}$ and $q_0 = 0$.

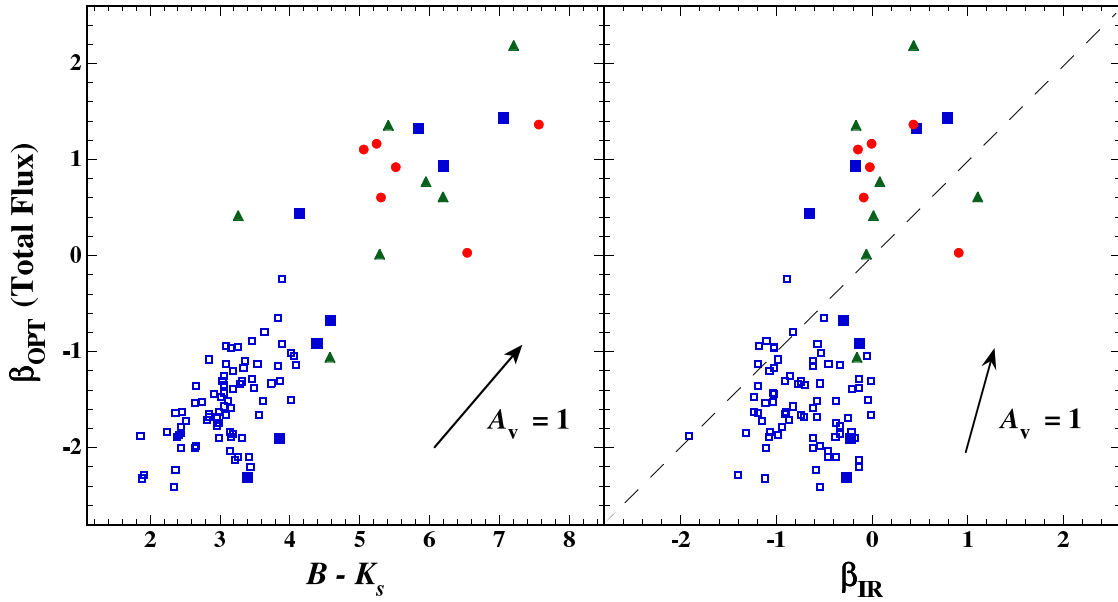


FIG. 6.— *Left Panel:* The spectral index of the power-law fits to the optical continua as a function of $B - K_s$ color index. *Right Panel:* Optical spectral index plotted against the spectral index of the power-law fits to the near-IR continua. The dashed line indicates $\beta_{\text{OPT}} = \beta_{\text{IR}}$. Symbols are the same as in Figure 5 for both panels. The near-IR and B -band data for the 2MASS QSOs are from the 2MASS Point Source Catalog. PG QSO data are from Neugebauer et al. (1987). For consistency with the PG QSOs data, no correction has been made for the stellar continuum of the host galaxy. A reddening vector of $A_V = 1$ is shown in both panels.

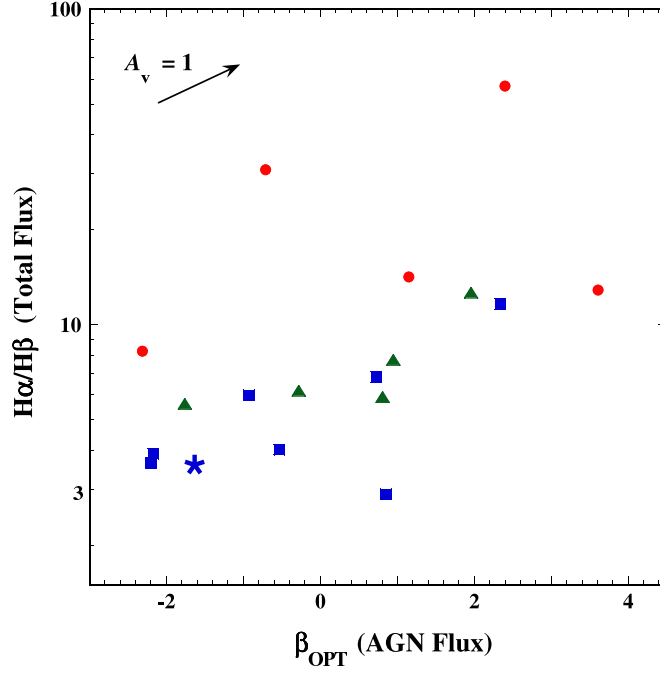


FIG. 7.— The Balmer decrement plotted against β_{OPT} for 17 2MASS QSOs in the spectropolarimetry survey. Starlight from the host galaxies of the 2MASS QSOs has been subtracted before fitting a power law to the continuum. It can be seen that in general the Balmer decrement is larger for objects with redder optical continua. Symbols are the same as in Figure 5. The *star* symbol marks the position of the median β_{OPT} for low-redshift PG QSOs and the Balmer decrement of the SDSS composite QSO. As in Figure 6, an $A_V = 1$ reddening vector is displayed.

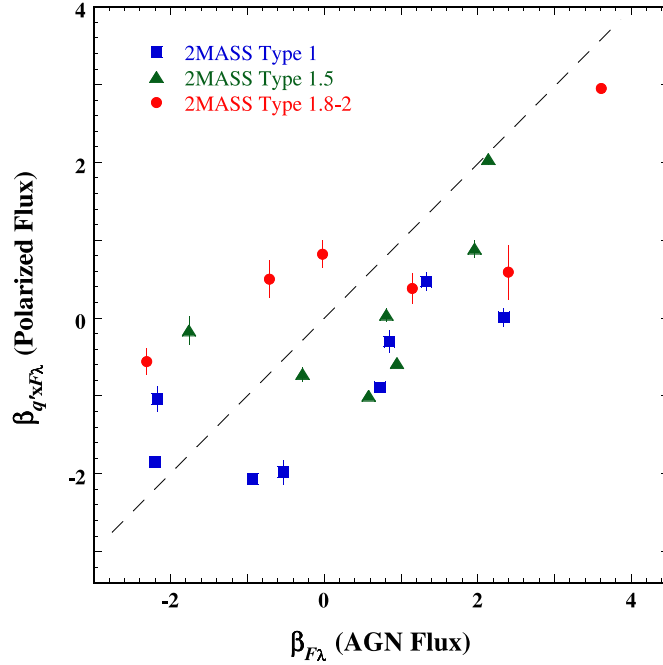


FIG. 8.— The spectral index of the polarized flux density spectrum plotted against the total flux density spectral index of the AGN component. The *dashed* line represents $\beta_{q \times F_\lambda} = \beta_{F_\lambda}$. Symbols are the same as in Figure 5. Error bars reflect the uncertainty in the power-law fits to the spectra, but do not include the uncertainties in the stellar spectra subtracted to yield the AGN spectra. This source of uncertainty is largest for the objects dominated by the light of the host galaxy; generally, the Type 1.8–2 QSOs.